An update to this article is included at the end

European Journal of Medicinal Chemistry 319 (2026) 119212

Contents lists available at ScienceDirect

European Journal of Medicinal Chemistry

journal homepage: www.elsevier.com/locate/ejmech

Research paper

Halogenated quinolinone–aziridines: Substituent-controlled diastereodivergent synthesis and geometry-dependent antiproliferative activity

Anđela Buljan [a], Marija Renić [a], Ana Čikoš [b], Višnja Stepanić [c], Karolina Begić Biškup [d], Mladen Paradžik [e], Marin Roje [a,*]

[a] Division of Organic Chemistry and Biochemistry, Scientific Center of Excellence for Marine Bioprospecting-BioProCro, Ruđer Bošković Institute, Bijenička cesta 54, Zagreb, 10000, Croatia
[b] NMR Centre, Ruđer Bošković Institute, Bijenička cesta 54, Zagreb, 10000, Croatia
[c] Division of Computing and Data Science, Ruđer Bošković Institute, Bijenička cesta 54, Zagreb, 10000, Croatia
[d] Division of Materials Chemistry, Ruđer Bošković Institute, Bijenička cesta 54, Zagreb, 10000, Croatia
[e] Division of Molecular Medicine, Ruđer Bošković Institute, Bijenička cesta 54, Zagreb, 10000, Croatia

ARTICLE INFO

Keywords:
Diastereodivergent synthesis
Fluorinated quinolinone-aziridines
Geometry-dependent activity
Structure-activity relationships
Selective antiproliferative activity
MCF-7 selectivity

ABSTRACT

A series of halogenated quinolinone-aziridine hybrids (±)-**14**–**20** inspired by marinoaziridine scaffolds was synthesized through an eight-step racemic route starting from two achiral fragments and convergently assembled *via* a sulfur ylide–imine aziridination reaction. The reaction afforded *cis* and *trans* aziridine derivatives in good yields (51–81%), with diastereoselectivity strongly dependent on the fluorine substitution pattern. Remarkably, complete stereoselectivity was observed for two derivatives, with the *meta*-fluorinated analogue (±)-**17** obtained exclusively as the *cis* isomer and the *di-ortho*-fluorinated analogue (±)-**19** exclusively as the *trans* isomer, highlighting the decisive role of substituent effects in controlling the stereochemical outcome of the reaction. The synthesized compounds were evaluated for antiproliferative activity against H460 and MCF-7 cancer cell lines and for cytotoxicity toward non-tumor HEK293T cells. Several derivatives displayed pronounced stereochemistry-dependent biological activity. In particular, selected *cis* isomers exhibited enhanced selectivity toward MCF-7 cells, whereas some *trans* analogues showed higher overall antiproliferative potency. Structure–activity relationship analysis revealed that both aziridine stereochemistry and fluorine substitution pattern play roles in determining biological response. Zebrafish embryotoxicity studies additionally demonstrated marked stereochemistry-dependent effects however with no direct correlation between antiproliferative selectivity and developmental toxicity. *In silico* target prediction suggested the possible involvement of proliferation-related signalling pathways, including kinase-associated targets. Overall, the results identify fluorine positioning is a critical determinant governing the stereochemical outcome of the synthesis, while both fluorine positioning and aziridine stereochemistry strongly influence antiproliferative activity, cellular selectivity, and embryotoxicity within this series of marine-inspired quinolinone–aziridine hybrids.

1. Introduction

The discovery and development of new bioactive molecules has been largely driven by the structural and functional diversity of natural products [1–4]. Natural products represent a major source of small-molecule drugs, semi-synthetic derivatives, and structural motifs that serve as a continuous source of inspiration for the development of new therapeutic agents [5–7]. However, their limited availability, particularly in the context of preserving newly discovered species, often restricts further derivatization and comprehensive biological evaluation [8]. In this context, laboratory replication of natural products combined with the rational design of derivatives represents a sustainable approach for exploring their biological potential [9,10].

Building on these considerations, we were particularly interested in

* Corresponding author.
E-mail addresses: Andjela.Buljan@irb.hr (A. Buljan), Ana.Cikos@irb.hr (A. Čikoš), Visnja.Stepanic@irb.hr (V. Stepanić), Karolina.Begic@irb.hr (K. Begić Biškup), Mladen.Paradzik@irb.hr (M. Paradžik), Marin.Roje@irb.hr (M. Roje).

https://doi.org/10.1016/j.ejmech.2026.119212
Received 18 June 2026; Received in revised form 31 July 2026; Accepted 3 August 2026
Available online 11 August 2026
0223-5234/© 2026 The Authors. Published by Elsevier Masson SAS. This is an open access article under the CC BY license (http://creativecommons.org/licenses/by/4.0/).

exploring marinoaziridines A and B, for which total synthesis has previously been achieved [11], as structural templates for the development of modified analogues. Interestingly, these compounds attracted our attention due to the presence of two pharmacophore relevant elements, an aziridine ring and a quinolinone core, which together form a hybrid molecular system with significant potential for structural optimization.

Aziridines are three-membered heterocyclic compounds whose reactivity arises from the combination of significant ring strain and polarization of the C–N bonds induced by the presence of a nitrogen atom [12–14]. This combination renders the aziridine ring susceptible to nucleophilic attack, leading to ring opening and enabling covalent interactions with biological targets [15]. The aziridine motif is found in numerous bioactive natural and synthetic compounds, where its biological activity is often associated with its ability to act as an alkylating agent in key biochemical processes [16]. Consequently, aziridines have attracted considerable interest in the development of bioactive, particularly anticancer agents [17].

On the other hand, quinolinones represent a well-established class of compounds widely present in biologically active molecules, known for their pronounced antiproliferative and antibacterial activities [18–20]. Considering the presence of these key pharmacophoric elements in marinoaziridines, we recognized their potential as a basis for the rational design of structurally modified derivatives aimed at optimizing biological properties.

In line with this approach, we designed a focused library of quinolinone–aziridine hybrids based on the marinoaziridine scaffold, by targeted structural modifications (Fig. 1). The original methyl groups were replaced with an aromatic moiety, introducing increased size, structural rigidity and a π-electron system, while enabling the incorporation of halogen substituents (*ortho*-, *meta*-, and *para*-) to modulate electronic and steric properties and potentially enhance interactions with biological targets. These modifications were designed to systematically investigate how the size, position and number of substituents control the stereochemistry and associated molecular conformation of the products, thereby governing geometry-dependent biological activity. Notably, we anticipated that subtle changes in substitution pattern could significantly influence the stereochemical outcome and, consequently, biological activity. In this context, we hypothesized that substitution pattern dictates the formation of specific *cis/trans* aziridine isomers, which define the spatial orientation of the aziridine moiety within the hybrid scaffold thereby governing its interaction with biological targets.

We devoted particular attention to fluorinated derivatives due to the unique physicochemical properties of fluorine [21–24]. As the smallest halogen, with a van der Waals radius of approximately 1.47 Å, fluorine is comparable in size to hydrogen (1.20 Å), allowing its incorporation without significant steric perturbation of the molecular framework. At the same time, its high electronegativity exerts a strong electron-withdrawing effect, which can significantly influence acidity and electron density distribution within the molecule. The introduction of fluorine enables modulation of key physicochemical parameters relevant to drug design, including lipophilicity, solubility, and binding affinity [25]. Furthermore, fluorine substitution affects conformational preferences and molecular recognition, thereby playing an important role in fine-tuning biological activity and ADME properties [26]. Within this framework, we investigated the influence of fluorine substitution, both in terms of position (*ortho*-, *meta*-, *para*-) and number of fluorine atoms on conformational properties and biological activity, with particular emphasis on the stereochemistry of the aziridine products (*cis/trans*) and geometry-dependent biological activity. For comparative evaluation of halogen effects, a *para*-chlorinated derivative was included, while the non-halogenated analogue served as a reference compound.

We retained the tosyl protecting group on the aziridine nitrogen to ensure stability during synthesis; however, it also represents a synthetic challenge in terms of its selective removal without ring opening. In addition, we introduced methyl substitution on the quinolinone moiety to modulate physicochemical properties, particularly solubility.

Herein, we report the synthesis of a series of halogenated quinolinone-aziridines inspired by marinoaziridines and evaluate their antiproliferative activity against selected human cancer cell lines, together with their embryotoxicity profile in the zebrafish model. Particular emphasis was placed on the influence of aromatic substitution and aziridine stereochemistry on biological activity. Structure-activity relationship (SAR) was analyzed and complemented by *in silico* target prediction and ADME analysis.

2. Results and discussion

2.1. Chemistry

To establish a viable synthetic route toward the target halogenated-quinolinone aziridines (±)-**14**–**20**, we first performed a retrosynthetic analysis (Scheme 1). Disconnection of the aziridine ring revealed two key precursors: the quinolinone-derived sulfonium salt **5** (ylide precursor 5′) and a series of *N*-tosyl imines **6**–**12** as electrophilic partners in the Johnson–Corey–Chaykovsky reaction [27]. This disconnection guided the design of a convergent synthetic strategy in which both fragments could be prepared independently and subsequently coupled to furnish the desired aziridine scaffold.

Halogenated quinolinone-aziridines (±)-**14**–**20** were synthesized through a convergent multistep sequence, as outlined in Scheme 2. The approach relied on the preparation of two key fragments prior to the Johnson–Corey–Chaykovsky reaction: a series of imines **6**–**12**, obtained from *p*-toluenesulfonamide and the corresponding aldehydes, and the

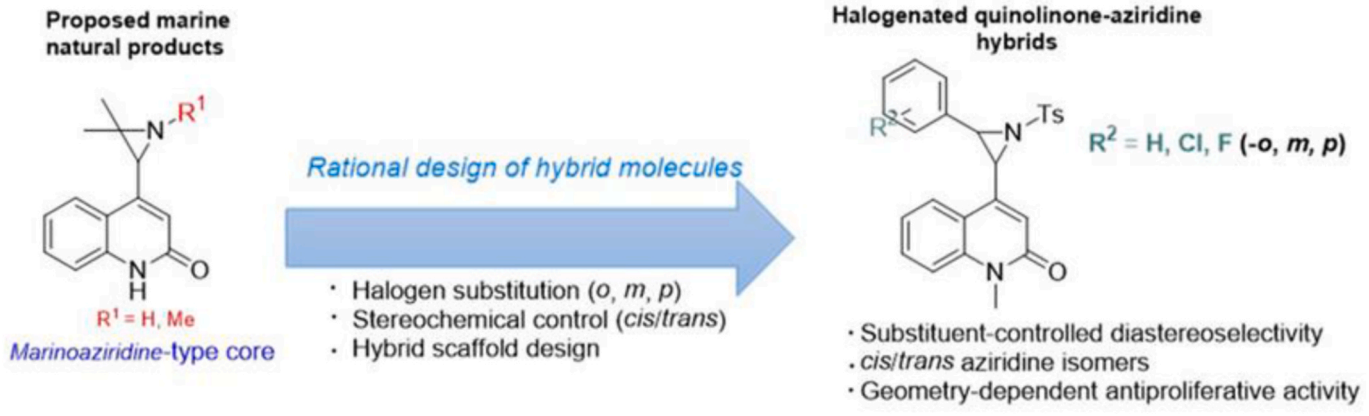

Fig. 1. Design strategy for halogenated quinolinone-aziridine hybrids based on a proposed marine natural product scaffold, highlighting systematic halogen substitution (R^2═H, Cl, F; *o*-, *m*-, *p*-).

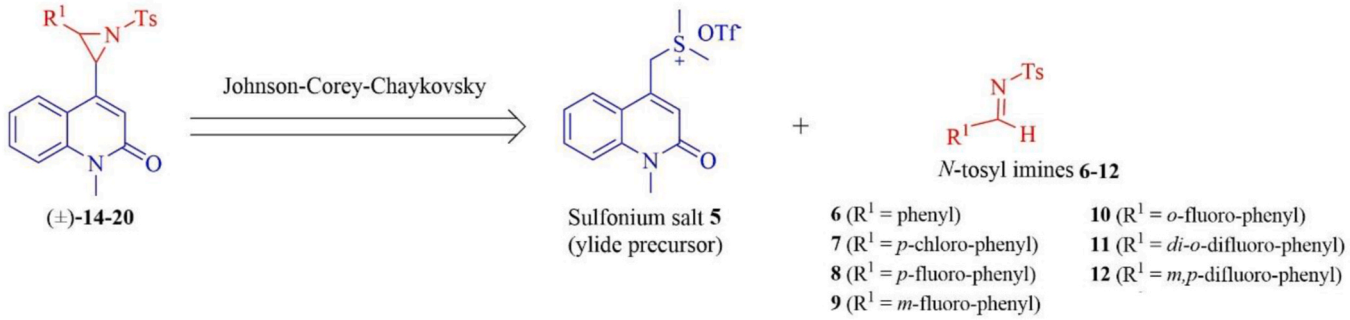

Scheme 1. Retrosynthetic analysis of halogenated quinolinone-aziridines (±)-**14**–**20**.

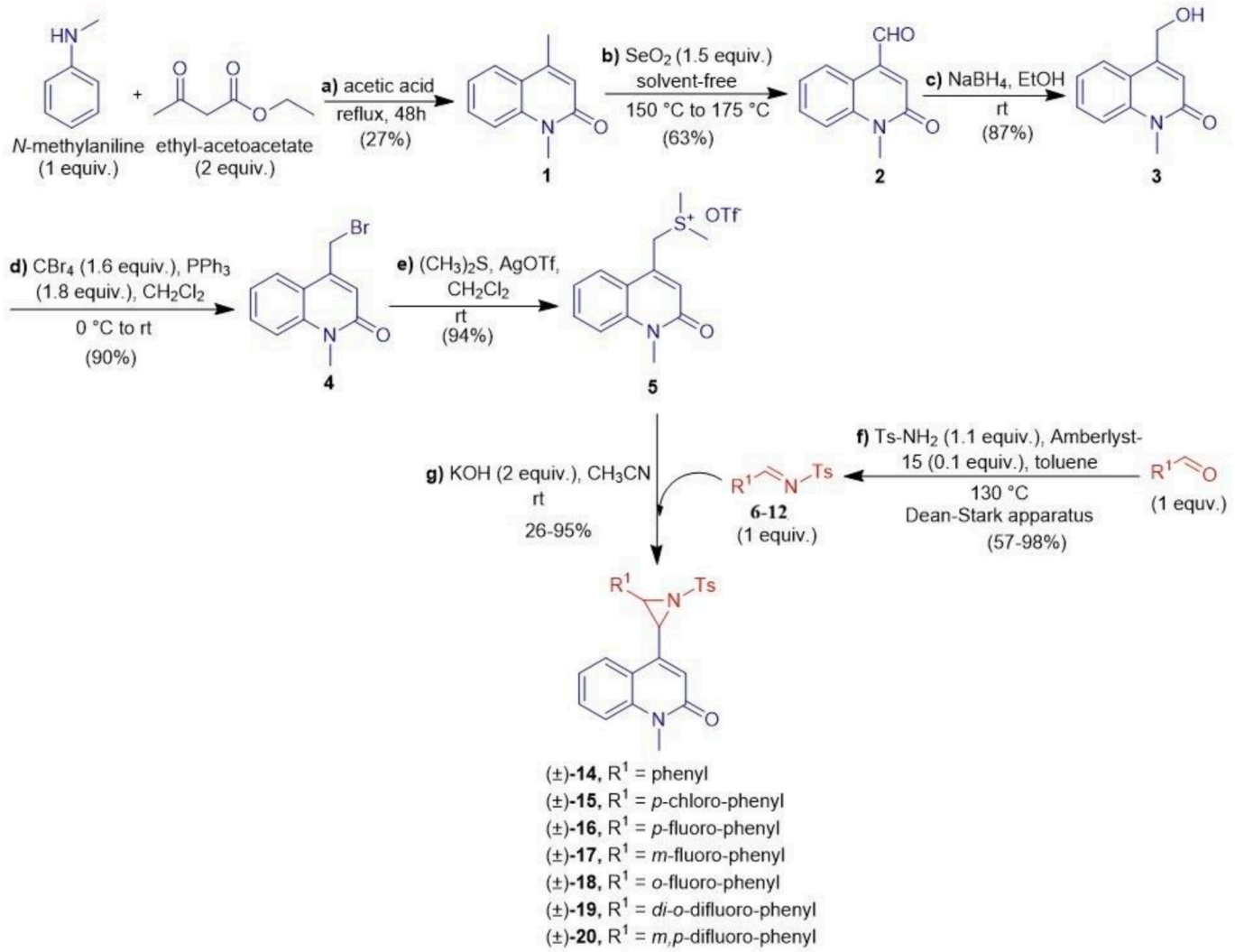

Scheme 2. The synthesis of halogenated quinolinone-aziridines (±)-**14**–**20**.

quinolinone-derived sulfur ylide precursor **5′**.

The synthesis of quinoline-2(1*H*)-one precursor **5** commenced with a well-established two-step Knorr-type reaction [28] starting from N-methylaniline and ethyl acetoacetate. In the first step, acetoacetanilide was formed and subsequently underwent *in situ* cyclization to afford quinoline-2(1*H*)-one **1** with complete regioselectivity in 40% yield. Oxidation of lactam **1** *via* the Riley reaction [29] furnished aldehyde **2** in 63% yield, which was then reduced with sodium borohydride ($NaBH_4$) to give alcohol **3** in 87% yield. Alcohol **3** was next subjected to Appel conditions [30] using carbon tetrabromide (CBr_4) and triphenylphosphine (PPh_3), affording bromide **4** in 90% yield. Finally, treatment of compound **4** with dimethyl sulfide and silver triflate (AgOTf) gave sulfonium salt **5** in 94% yield as the key ylide precursor.

In parallel, imines **6**–**12** were prepared by condensation of equimolar amounts of *p*-toluenesulfonamide and the corresponding aldehydes using Amberlyst®-15 under Dean–Stark conditions. Most imines contained minor amounts of residual *p*-toluenesulfonamide ($TsNH_2$), as indicated by additional signals in their ^1H and ^{13}C NMR spectra.

Following recrystallization, this impurity persisted in six cases, while compounds **6** and **8** were obtained in higher purity.

With both fragments **5** and **6**–**12** in hand, halogenated quinolinone-aziridines (±)-**14**–**20** were obtained through the reaction of the *in situ* generated sulfur ylide **5′** with *N*-tosyl imines **6**–**12**. Cyclization in the presence of potassium hydroxide (KOH) afforded the desired racemic *cis* and/or *trans* aziridine isomers in yields ranging from 51 to 81%. In several cases (±)-**15**, (±)-**16**, (±)-**18** and (±)-**20**, chromatographic purification enabled the isolation of both *cis* and *trans* isomers. In contrast, derivative (±)-**17** was obtained exclusively as the *cis* isomer, whereas derivative (±)-**19** was formed exclusively as the *trans* isomer. For compound (±)-**14**, both *cis* and *trans* isomers were detected by ^{1}H NMR analysis, with the *trans* isomer predominating in the crude mixture. However, only the *trans* isomer was successfully isolated and further characterized.

2.2. Diastereoselectivity and stereochemical analysis

To reliably assign the stereochemistry, a representative aziridine sample ((±)-**15**), obtained as a mixture of two diastereomers (ca. 11:9 ratio), was subjected to detailed 1D and 2D NMR analysis (Fig. S28–S39). It should be noted that this ratio reflects the composition of the analyzed sample after partial isolation of the *trans* isomer, and not the original diastereomeric ratio; in the crude reaction mixture, compound (±)-**15** was typically obtained in a *trans*/*cis* ratio of approximately 4:1. Key NOE contacts enabled unambiguous assignment of the relative configurations. The major component (ca. 55%) was identified as the *trans* isomer (*RR*, *SS*, or a mixture of *RR* and *SS* isomers) based on a characteristic vicinal coupling constant ($^3J_{H\text{-}12,H\text{-}14} = 4.6$ Hz) and a network of NOE contacts. Spatial correlations between H-12 and H-16,20 indicate that these protons are oriented towards one face of the aziridine ring, while NOE interaction between H-14 and H-2 suggests that H-14 is facing the opposite direction (Fig. 2a), thus giving evidence of the overall aziridine configuration being *trans*. In contrast, the minor component (ca. 45%) was assigned as the *cis* isomer, (*RS*, *SR*, or a mixture of *RS* and *SR* isomers), displaying a larger coupling constant ($^3J_{H\text{-}12,H\text{-}14} = 7.3$ Hz) and crucial NOE contact between H-2 and H-16,20, consistent with benzene ring and quinolinone functionalities facing the same direction making the overall aziridine configuration *cis* (Fig. 2b).

Based on these experimentally established correlations, characteristic coupling constants were used as a reliable diagnostic tool for stereochemical assignment. *Cis* isomers exhibited larger coupling constants (7.1–7.6 Hz), whereas *trans* isomers showed lower values (4.1–4.8 Hz) (see Supporting Information, Table S1). These criteria were subsequently applied to assign the stereochemistry of all derivatives directly from their ^{1}H NMR spectra, including crude reaction mixtures (see Supporting Information, Fig. S21–S27).

Application of these criteria across the entire series revealed a clear and consistent trend in diastereoselectivity, with the *trans* isomer predominating in most cases under the applied reaction conditions (Table 1).

Particularly notable are derivatives (±)-**17** and (±)-**19**, which exhibited complete diastereoselectivity, being obtained exclusively as the *cis* and *trans* isomers, respectively. This complete stereocontrol highlights the decisive role of substituent effects in directing the reaction outcome.

The observed diastereoselectivity can be rationalized by a Curtin–Hammett scenario involving a zwitterionic betaine intermediate (Scheme 3) [31,32]. In this context, the stereochemical outcome is governed by substituent-dependent steric and electronic effects that influence the relative accessibility of competing reaction pathways.

In particular, comparison of the *meta*-fluorinated (±)-**17** and *di-ortho*-fluorinated systems (±)-**19** suggests that the position of the fluorine substituent plays a key role in directing the reaction outcome. The exclusive formation of the *cis* isomer for the *meta*-fluorinated derivative (±)-**17** may be attributed to the absence of steric hindrance near the reaction center, which allows access to the *cis*-forming pathway. In this position, fluorine exerts predominantly an inductive effect without

Table 1
Diastereomeric ratios (*cis*/*trans*) of halogenated quinolinone-aziridines (±)-**14**–**20** determined by ^{1}H NMR analysis of crude reaction mixtures, together with the predominant and isolated isomers obtained after chromatographic purification.

Compound	*cis*/*trans* ratio[a]	Major isomer	Isolated isomer
(±)-**14**	14/86	*trans*	*trans*
(±)-**15**	20/80	*trans*	*trans* + *cis* (*separated*)[b]
(±)-**16**	18/82	*trans*	*trans* + *cis* (*separated*)[b]
(±)-**17**	100/0	*cis*	*cis*
(±)-**18**	21/79	*trans*	*trans* + *cis* (*separated*)[b]
(±)-**19**	0/100	*trans*	*trans*
(±)-**20**	14/86	*trans*	*trans* + *cis* (*separated*)[b]

[a] Determined from ^{1}H NMR analysis of crude reaction mixtures.
[b] Both isomers were isolated by column chromatography.

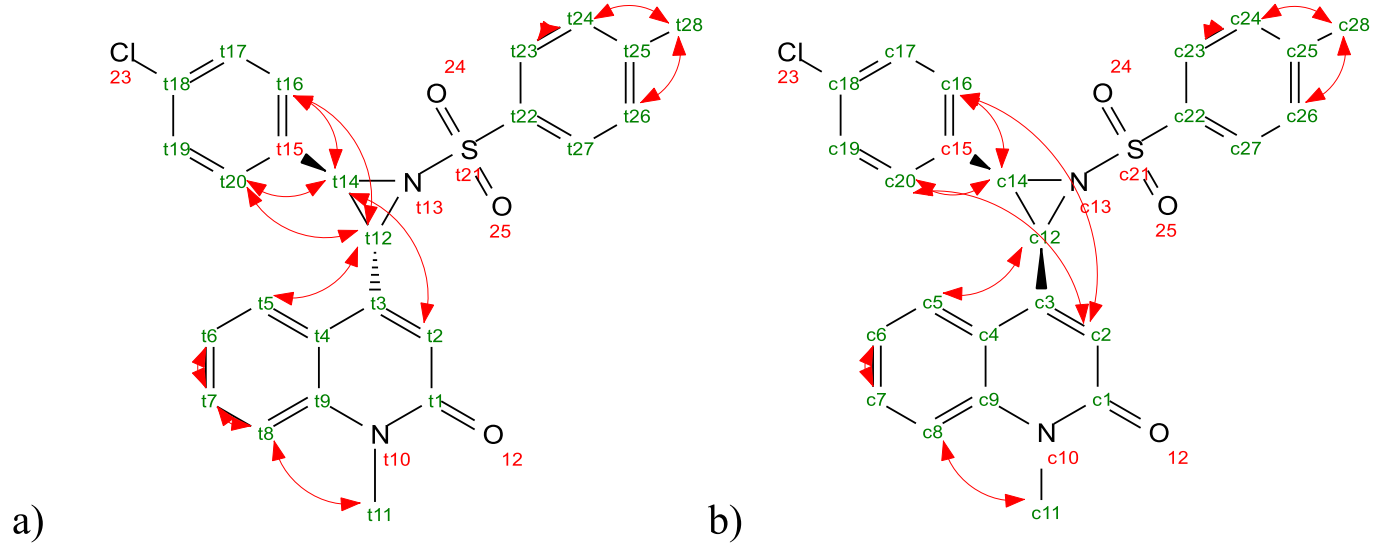

Fig. 2. Structures, numbering and key NOE contacts (red arrows) for a) *trans* and b) *cis* component of (±)-**15** in $CDCl_3$ at 25 °C (only one enantiomer shown for clarity).

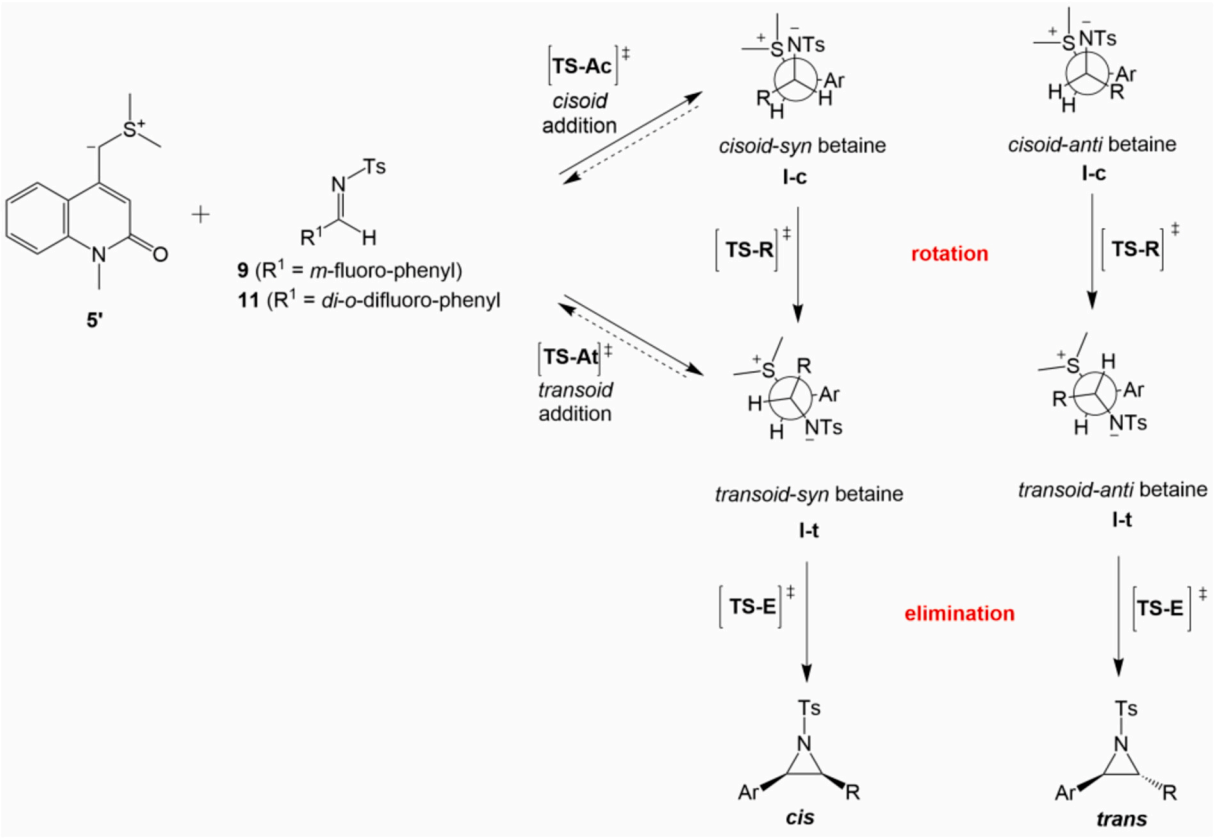

Scheme 3. Generally accepted mechanism for aziridine formation from sulfur ylide and aldimines.

direct resonance interaction, and therefore does not impose additional electronic constraints on the reaction outcome. In contrast, increased steric congestion in the *di-ortho*-fluorinated system (±)-**19** restricts conformational flexibility and favors formation of the *trans* isomer, with possible additional contributions from position-dependent electronic effects, including resonance interactions.

2.3. Biological evaluation

The synthesized halogenated quinolinone-aziridines (±)-**14**–**20** were evaluated for their biological activity to assess the impact of structural variations on their pharmacological properties. Prior to biological testing, all compounds were purified to ≥ 98% as determined by HPLC (see Supporting Information, Table S2, Fig. S62–S72) and dried under high vacuum. In several cases, both *cis* and *trans* diastereomers were isolated and evaluated separately ((±)-**15**, (±)-**16**, (±)-**18**, (±)-**20**), enabling assessment of the influence of stereochemistry on biological activity. For compound (±)-**14**, the major *trans* isomer was selected for biological evaluation, as it could be obtained in pure form. The biological evaluation included antiproliferative activity against selected human cancer cell lines and zebrafish embryotoxicity assessment.

2.3.1. Antiproliferative activity

The antiproliferative activity was evaluated against two human cancer cell lines, MCF-7 (breast cancer) and H-460 (lung cancer), while HEK293T (human embryonic kidney) cells were used as a non-tumor control. The results of these assays are summarized in Table S3.

Overall, the tested compounds exhibited moderate to good antiproliferative activity, with clear dependence on both the aromatic substitution pattern and aziridine stereochemistry.

Trans isomers generally displayed higher cytotoxicity compared to their *cis* counterparts, although several *cis* isomers showed improved selectivity toward MCF-7 cells. Among the series, compound (±)-*trans*-**20** showed the highest activity across all tested cell lines, with an IC_{50} values in the low micromolar range. However, this compound also exhibited comparable cytotoxicity toward HEK293T cells, indicating limited selectivity.

These results are further discussed in the SAR section.

2.3.2. Zebrafish toxicity

The embryotoxic potential of the synthesized compounds was evaluated using *Danio rerio* embryos. Eleven samples were assessed: (±)-*trans*-**14**, (±)-*trans*-**15**, (±)-*trans*-**16**, (±)-*trans*-**18**, (±)-*trans*-**19**, (±)-*trans*-**20**, (±)-*cis*-**15**, (±)-*cis*-**16**, (±)-*cis*-**17**, (±)-*cis*-**18**, *and* (±)-*cis*-**20**. Half-maximal lethal concentrations (LC_{50}; Table S4) were extrapolated from the concentration–response curves presented in Fig. S73. Notable differences in embryotoxicity were observed among the evaluated *cis/trans* pairs, indicating that stereochemistry plays an important role in determining the toxicity profile of these compounds. Particularly pronounced stereochemistry-dependent effects were observed for compounds (±)-**15** and (±)-**20**. While (±)-*cis*-**15** and (±)-*cis*-**20** exhibited LC_{50} values 0.0043 and 0.0041 mg/mL, respectively, the corresponding *trans* isomers did not reach LC_{50} within the tested concentration range. LC_{50} values for (±)-*trans*-**15**, (±)-*trans*-**20**, and (±)-*cis*-**18** were not reached within the tested concentration range, with maximal mortality limited to 20% at the highest tested concentrations. Notably, (±)-*trans*-**19** and (±)-*cis*-**17** showed no observable adverse effects on embryo survival across the tested concentration range, suggesting a favorable *in vivo* safety profile. Compound (±)-*cis*-**20** demonstrated the highest toxicity, with the lowest LC_{50} value (0.0041 mg/mL; 95% CI: 0.0035 - 0.0048). The lethality observed in the negative control group was below 5%.

2.4. Structure-activity relationship (SAR) and stereochemical effects

Analysis of the structure–activity relationships within the prepared

series of halogenated quinolinone-aziridines (±)-**14**–**20** clearly indicates that the stereochemistry of the aziridine ring plays a crucial role not only in determining antiproliferative potency but also in modulating cellular selectivity. While several *trans* isomers displayed higher overall activity, particularly against the H460 lung cancer cell line, the most notable observation was the preferential activity of selected *cis* derivatives toward MCF-7 breast cancer cells combined with reduced toxicity toward the non-tumor HEK293T cell line (Fig. 3).

The non-fluorinated reference compound (±)-*trans*-**14** displayed comparable antiproliferative activity against all three tested cell line (GI_{50} = 9.4–13.7 μM), indicating limited selectivity. This profile provides an important baseline for evaluating the impact of fluorine substitution and aziridine stereochemistry on biological activity. In comparison with the reference scaffold, several fluorinated *cis* derivatives exhibited markedly improved selectivity toward MCF-7 cells, while maintaining reduced toxicity toward HEK293T cells.

The clearest example of stereochemistry-dependent selectivity is observed for compound (±)-**15** (Fig. 4). While (±)-*trans*-**15** displayed moderate activity against both H460 ($GI_{50} = 22.6 \pm 5.7$ μM) and MCF-7 cells ($GI_{50} = 13.8 \pm 0.2$ μM), together with comparable toxicity toward HEK293T cells ($GI_{50} = 22.4 \pm 6.8$ μM), the corresponding (±)-*cis*-**15** exhibited a markedly different biological profile. The *cis* isomer retained good activity against MCF-7 cells ($GI_{50} = 9.5 \pm 3.3$ μM) while being essentially inactive toward both H460 and HEK293T cells ($GI_{50} > 100$ μM), indicating a pronounced preference for the breast cancer cell line.

An additional interesting observation is provided by compound (±)-**16**, where both diastereomers display activity exclusively toward MCF-7 cells, while remaining inactive against H460 and HEK293T cell lines. In this case, the *trans* isomer shows somewhat higher activity ($GI_{50} = 11.3 \pm 1.9$ μM) than the corresponding *cis* analogue ($GI_{50} = 19.4 \pm 8.8$ μM), indicating a pronounced preference of this scaffold for the MCF-7 cell line.

The diastereomeric pair of compound (±)-**20** is particularly illustrative. The *trans* isomer, (±)-*trans*-**20**, is among the most potent compounds in the series, displaying strong antiproliferative activity against all tested cell lines ($GI_{50} = 3.9 \pm 0.5$ μM for H460; 4.0 ± 2.4 μM for MCF-7; 3.6 ± 0.5 μM for HEK293T). However, its comparable cytotoxicity toward the non-tumor HEK293T cell line indicates limited selectivity. In contrast, the corresponding *cis* isomer, (±)-*cis*-**20**, shows a markedly different activity profile. It is essentially inactive toward H460 cells ($GI_{50} > 100$ μM), while retaining good activity against MCF-7 cells ($GI_{50} = 6.6 \pm 0.8$ μM), along with substantially reduced cytotoxicity toward HEK293T cells ($GI_{50} = 56.5$ μM). This shift points to a more favorable biological profile for the *cis* isomer, with a clear preference for MCF-7 cells, and further emphasizes the importance of stereochemistry in modulating biological response.

Further analysis reveals that both the number and the position of fluorine substituents have a significant impact on biological activity. Comparison of the monosubstituted derivatives (±)-**16**–**18** shows that changing the position of a single fluorine atom leads to substantial differences in activity. The *para*-fluorinated derivative (±)-**16** exhibits a clear preference for MCF-7 cells, the *meta*-fluorinated derivative (±)-**17** shows weaker activity, while the *ortho*-fluorinated derivative (±)-**18** displays increased potency, but also higher cytotoxicity toward HEK293T cells.

The importance of substituent positioning is further highlighted by comparison of the difluorinated derivatives (±)-*trans*-**19** and (±)-*trans*-**20**. Although both compounds contain two fluorine atoms, the *di-ortho*-fluorinated derivative (±)-*trans*-**19** shows a pronounced loss of activity ($GI_{50} = 87.6 \pm 9.7$ μM for H460; >100 μM for MCF-7 and HEK293T), whereas the *meta/para*-substituted derivative (±)-*trans*-**20** exhibits the highest activity in the series. These findings clearly demonstrate that the position of fluorine substituents exerts a much stronger influence on biological activity than fluorine content alone.

The zebrafish embryotoxicity data further emphasized the importance of aziridine stereochemistry in shaping the biological profile of this compound series. Interestingly, no direct correlation was observed between antiproliferative activity, cellular selectivity, and embryotoxicity. For example, the highly selective MCF-7-active derivatives (±)-*cis*-**15** and (±)-*cis*-**20** exhibited pronounced embryotoxicity, whereas (±)-*trans*-**19** and (±)-*cis*-**17** showed no observable adverse effects on embryo survival within the tested concentration range. These findings suggest that the structural features governing cancer cell selectivity and

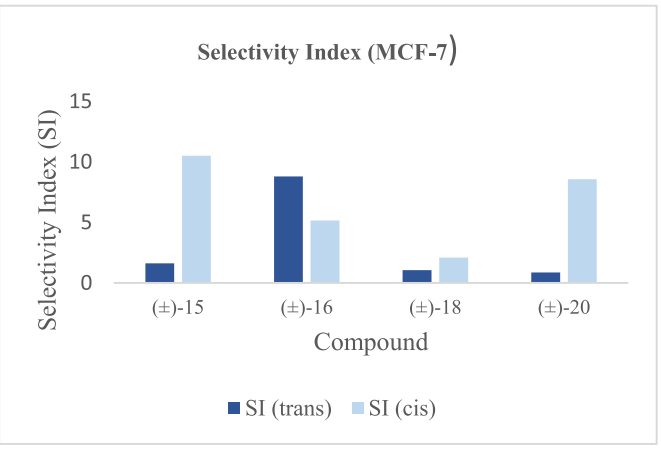

Fig. 4. Selectivity index (SI) values for selected *cis/trans* diastereomeric pairs ((±)-**15**, (±)-**16**, (±)-**18**, and (±)-**20**) against MCF-7 cells. The selectivity index was calculated as the ratio of GI_{50} values for HEK293T and MCF-7 cell lines (SI = GI_{50} HEK293T/GI_{50} MCF-7).

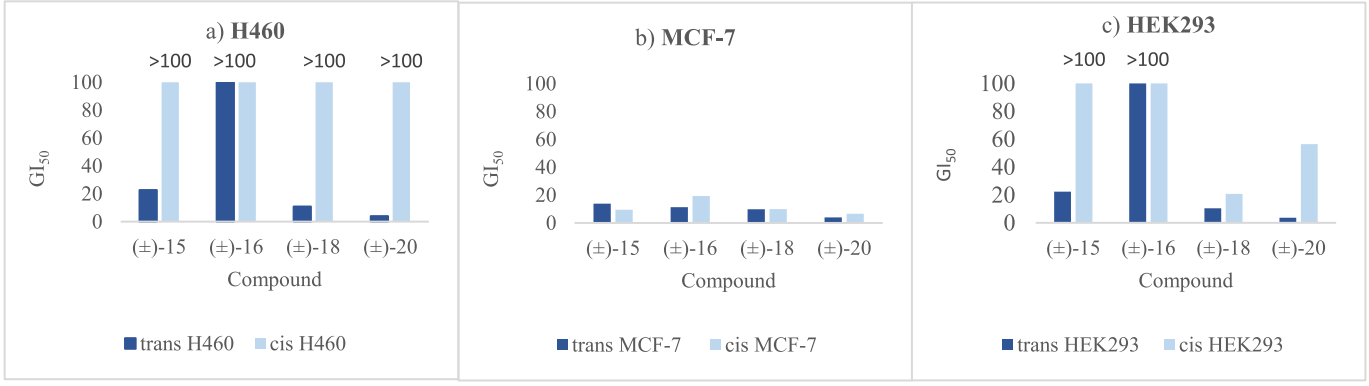

Fig. 3. Influence of aziridine stereochemistry on antiproliferative activity. Comparison of GI_{50} values for selected *cis/trans* diastereomeric pairs ((±)-**15**, (±)-**16**, (±)-**18**, and (±)-**20**) against (a) H460, (b) MCF-7, and (c) HEK293T cell lines. Values > 100 μM are capped at 100 μM for clarity.

developmental toxicity are at least partially distinct, highlighting the complex role of both fluorine substitution pattern and aziridine stereochemistry in determining the overall biological profile.

According to the *in silico* ADME predictions obtained at SwissADME server (Table S5), all derivatives are predicted to have similar ADME profile characterized by high gastrointestinal absorption, whereas lipophilicity increases with the introduction of halogen substituents [33]. This increase may influence membrane permeability and may also be associated with higher cytotoxicity and reduced selectivity, as observed for difluorinated derivatives. The predicted ADME profiles of the *cis* and *trans* diastereoisomeric pairs were identical. Most compounds comply with Lipinski's rule of five without any violations, whereas the difluorinated derivatives ((±)-**19**,**20**) show a single predicted violation, while still maintaining favorable overall pharmacokinetic profiles.

Taken together, these results indicate that aziridine stereochemistry primarily modulates cellular selectivity and embryotoxicity, whereas fluorine substitution pattern governs both stereochemical outcome and measured biological activity. Several *cis* derivatives, particularly (±)-*cis*-**15**, (±)-*cis*-**18** and (±)-*cis*-**20**, displayed a favorable selectivity profile toward MCF-7 cells, while the comparison of (±)-*trans*-**19** and (±)-*trans*-**20** highlights the critical importance of fluorine positioning in determining antiproliferative activity. The zebrafish data further suggest that antiproliferative selectivity and embryotoxicity are not directly correlated, indicating that distinct structural features may govern different biological responses.

2.5. In silico target prediction

To gain preliminary insight into the possible mechanisms of actions underlying the observed antiproliferative activity, *in silico* target prediction analyses were performed using Swiss Target Prediction webserver and PASS commercial software [34,35]. Swiss Target Prediction revealed several commonly predicted protein targets associated with signalling and proliferation-related pathways, including kinase-associated proteins such as MET receptor tyrosine kinase, together with phosphodiesterases and prenyltransferase-related targets. Importantly, several of these predicted targets are biologically relevant in the context of MCF-7 breast cancer cells and cellular proliferation pathways.

In parallel, PASS analysis suggested activities associated with kinase-related signalling, including Ca2+/calmodulin-dependent kinase, MAP kinase and cyclin-dependent kinase-related pathways, together with antineoplastic and apoptosis-associated activities. Although these predictions do not represent direct evidence of a specific molecular target, the consistency between Swiss Target Prediction and PASS analyses supports the possible involvement of proliferation-associated signalling mechanisms in the observed biological effects.

Particularly interesting was the observed difference in biological activity between cis and trans isomers. The distinct three-dimensional arrangement of these stereoisomers may lead to different binding orientations and interaction patterns within biologically relevant targets, potentially contributing to the observed geometry-dependent selective antiproliferative activity toward MCF-7 cells.

3. Materials and methods

3.1. Synthesis

All synthetic procedures were conducted under an inert argon atmosphere unless noted otherwise. Solvents employed were either of analytical grade (puriss. p.a.) or freshly distilled over suitable drying agents. Glassware was pretreated either by flame-drying under reduced pressure or by heating in an oven at 120 °C for at least 12 h prior to use. Reactions involving air- or moisture-sensitive reagents were handled using syringe techniques. Commercially available reagents were used as supplied without further purification. Flash column chromatography was performed on silica gel (Fluka Analytical, particle size 35–75 μm). Reaction monitoring was carried out using thin-layer chromatography (TLC) on precoated silica plates (DC-Alufolien-Kieselgel F254, Sigma-Aldrich), with detection under UV light at 254 nm.

3.2. General methods

All solvents used for NMR sample preparation were purchased from EurIsotop (Saint-Aubin, France). The complete ^{1}H and ^{13}C assignments were made on the basis of one- and two-dimensional NMR spectra (^{1}H, ^{13}C, COSY, NOESY, HSQC and HMBC). All spectra were recorded on Bruker Avance AV600 equipped with 5 mm diameter BBO probe with *z*-gradient accessory. Spectra were acquired using standard Bruker pulse sequences, detailed experimental parameters can be found in Supplementary Material. All samples were dissolved in $CDCl_3$ or DMSO-d_6, while TMS was used as internal standard for referencing. NOESY spectra were obtained with the mixing time of 500 ms. Signal multiplicities are reported using the following abbreviations: br – broad, s – singlet, d – doublet, t – triplet, q – quartet, m – multiplet.

Melting points were measured in open capillaries on an Electrothermal 9100 melting point apparatus and are reported without correction.

High-resolution mass spectra (HRMS) were acquired using an Agilent 6545 LC/Q-TOF mass spectrometer in positive electrospray ionization (ESI) mode. Samples were prepared in methanol/acetonitrile (9:1) and introduced directly into the detector using a mobile phase consisting of 70% acetonitrile with 0.1% formic acid and 30% water with 0.1% formic acid, at a flow rate of 0.2 mL min^{-1}. Data acquisition and analysis were performed using Agilent MassHunter software.

3.3. Experimental section

3.3.1. Preparation of sulfonium salt *5*

The compounds **1** and **2** were synthesized to following our reported procedure [36].

3.3.1.1. Preparation of 4-(hydroxymethyl)-1-methylquinolin-2(1H)-one *3*

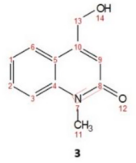

3

To a suspension of aldehyde **2** (1.16 g, 6.20 mmol) in ethanol (50 mL), sodium borohydride (0.47 g, 12.4 mmol) was added. The reaction mixture was stirred at room temperature for 2 h, until HPLC indicated complete consumption of starting materials. The reaction was quenched by the addition of ammonium chloride (15 mL). The aqueous layer was extracted with ethyl acetate (3 x 20 mL). The combined organic layers were washed with brine, dried over anhydrous Na_2SO_4, filtered and concentrated under reduced pressure. The crude product was purified *via* column chromatography (*flash* silica gel, dichloromethane/methanol = 25/1). Pure product **3** was obtained as a white solid (1.01 g, 87% yield).

Data for 4-(hydroxymethyl)-1-methylquinolin-2(1*H*)-one 3: a white solid, m.p. 135 – 136.5 °C; ^{1}H NMR (300 MHz, Chloroform-*d*) δ/ppm: 3.64 (s, 3H, H-11), 4.95 (s, 2H, H-13), 6.87 (s, 1H, H-9), 7.22 – 7.30 (m, 1H, H-3), 7.34 (d, $J_1 = 8.5$ Hz, 1H, H-1), 7.58 (ddd, $J_1 = 1.2$ Hz, $J_2 = 7.4$ Hz, $J_3 = 8.5$ Hz, 1H, H-2), 7.72 (dd, $J_1 = 1.5$ Hz, $J_2 = 8.0$ Hz, 1H, H-6).

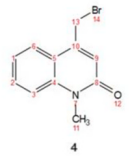

4

*3.3.1.2. Preparation of 4-(bromomethyl)-1-methylquinolin-2(1H)-one **4**.* A mixture of alcohol **3** (1.01 g, 5.40 mmol) and tetrabromomethane (2.84 g, 8.63 mmol) in dry dichloromethane (500 mL) was cooled to 0 °C under an atmosphere of argon. To this mixture, triphenylphosphine (2.52 g, 9.71 mmol) was added and resulting mixture was stirred at that temperature for 1 h. The reaction was then warmed to room temperature and was stirred for 20 h until HPLC indicated complete consumption of starting materials. The volatiles were removed under reduced pressure. The crude product was purified *via* column chromatography (*flash* silica gel, dichloromethane/methanol = 25/1). Pure product **4** was obtained as a light yellow solid (1.22 g, 90% yield).

Data for 4-(bromomethyl)-1-methylquinolin-2(1*H*)-one 4: a light yellow solid; m.p. 144.4 – 149.9 °C; ^{1}H NMR (600 MHz, Chloroform-*d*) δ/ppm: 3.73 (s, 3H, H-11), 4.58 (s, 2H, H-13), 6.82 (s, 1H, H-9), 7.33 (ddd, $J_1 = 1.0$ Hz, $J_2 = 7.2$ Hz, $J_3 = 8.1$ Hz, 1H, H-3), 7.42 (m, 1H, H-1), 7.62 (ddd, $J_1 = 1.4$ Hz, $J_2 = 7.2$ Hz, $J_3 = 8.6$ Hz, 1H, H-2), 7.85 (dd, $J_1 = 1.4$ Hz, $J_2 = 8.0$ Hz, 1H, H-6); ^{13}C (151 MHz, Chloroform-*d*) δ/ppm 28.2 (C-11), 29.5 (C-13), 114.85 (C-9), 118.6 (C-3), 122.2 (C-1), 122.2 (C-5), 125.2 (C-6), 131.1 (C-2), 140.4 (C-4), 144.6 (C-10), 161.6 (C-8); IR $\tilde{\nu}_{max}$/cm^{-1}: 3071; 3028; 2973; 1662; 1641; 1587; 1504; 1563; 1450; 1396; 1323; 1213; 751; 717; HRMS *m/z* 252.00268 (calculated for $C_{11}H_{10}BrNO$ $[M+H]^+$.

*3.3.1.3. Preparation of dimethyl((1-methyl-2-oxo-1,2-dihydroquinolin-4-yl)methyl)sulfonium triflate **5***

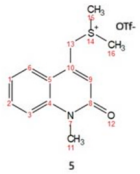

5

To a mixture of bromide **4** (1.22 g, 4.84 mmol) and dimethyl sulfide (0.43 mL, 5.81 mmol) in dry dichloromethane (20 mL) AgOTf (1.24 g, 4.84 mmol) was added at room temperature under an atmosphere of argon. The mixture was covered with aluminium foil. The solution turned grey and a grey solution started to precipitate, and then the resulting mixture was stirred 24 h, until TLC indicated complete consumption of starting materials. The volatiles were removed under reduced pressure. The reaction mixture was dissolved in DMSO and the resulting suspension was filtered through a short pad of Celite. The filtrate was concentrated *in vacuo* to give a yellow oil. After being washed with ether, the residue was dried under reduced pressure and recrystallized from diethyl ethere to provide the sulfonium salt **5** (1.73 g, 94% yield) as a white solid.

Data for dimethyl((1-methyl-2-oxo-1,2-dihydroquinolin-4-yl) methyl)sulfonium triflate 5: a white solid; m.p. 184.2 – 186.6 °C; ^{1}H NMR (300 MHz, Dimethyl sulfoxide-*d6*) δ/ppm 2.95 (s, 6H, H-15,16), 3.65 (s, 3H, H-11), 4.87 (s, 2H, H-13), 6.86 (s, 1H, H-9), 7.34 – 7.44 (m, 1H, H-3), 7.64 (d, $J_1 = 8.4$ Hz, 1H, H-1), 7.69 – 7.79 (m, 1H, H-2), 8.12 (dd, $J_1 = 0.8$ Hz, $J_2 = 8.0$ Hz, 1H, H-6); ^{13}C (75 MHz, Dimethyl sulfoxide-*d6*): 24.9 (2C, C-15,16), 29.2 (C-11), 42.7 (C-13), 115.5 (C-3), 118.4 (C-9), 122.2 (C-1), 125.1 (C-5), 125.2 (C-6), 131.7 (C-2), 137.3 (C-10), 140.1 (C-4), 159.9 (C-8); IR $\tilde{\nu}_{max}$/cm^{-1}: 3430; 3020; 2994; 2951; 1647; 1588; 1562; 1506; 1455; 1258; 1154; 1023; 760; 632.

*3.3.2. Preparation of N-tosylimines **6–13***

General procedure for preparation of *N*-Ts aldimines 6–13: To a round-bottom flask equipped with a Dean-Stark trap were added the corresponding aldehyde (1 equiv.), *p*-toluenesulfonamide (1.1 equiv.), and Amberlist®-15 (10 mol%) in dry toluene under an atmosphere argon. The reaction mixture was refluxed for 24 h under argon until TLC analysis indicated complete consumption of starting materials. The mixture was cooled to room temperature, and the resulting dark-orange suspension was filtered through a short pad of Celite. The filtrate was concentrated *in vacuo* to give a crude product, which was purified by recrystallization from dichloromethane/hexane, (9/1) to afford the desired *N*-tosyl-aldimine as a white solid.

*3.3.2.1. Preparation of (E)-N-benzylidene-4-methylbenzenesulfonamide **6***

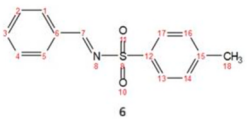

6

According to the general procedure, starting from benzaldehyde (0.48 mL, 4.71 mmol), *p*-toluenesolfonamide (0.81 g, 4.71 mmol) and Amberlist®-15 in dry toluene (20 mL), compound **6** (0.69 g, 57%) was obtained as a white solid.

Data for (*E*)-*N*-benzylidene-4-methylbenzenesulfonamide 6: a white solid, ^{1}H NMR (300 MHz, Chloroform-*d*) δ/ppm 2.45 (s, 3H, H-18), 7.36 (d, $J_1 = 8.0$ Hz, 2H, H-14,16), 7.50 (t, $J_1 = 7.6$ Hz, 2H, H-2,3), 7.64 (dd, $J_1 = 6.2$ Hz, $J_2 = 8.5$ Hz, 1H, H-4), 7.93 (dd, $J_1 = 7.9$ Hz, $J_2 = 9.9$ Hz, 4H, H-13,17,1,5), 9.05 (s, 1H, H-7); ^{13}C (75 MHz, Chloroform-*d*) δ/ppm 24.6 (C-18), 128.1 (2C, C-1,5), 129.2 (2C, C-13,17), 129.8 (2C, C-2,4), 131.3 (2C, C-16,14), 132.4 (C-6), 134.9 (C-3), 135.17 (C-12), 144.6 (C-15), 170.1 (C-7); IR $\tilde{\nu}_{max}$/cm^{-1}: 3071, 1650, 1596, 1574, 1450, 1317, 1305, 1223, 1155, 1086, 867, 781.

*3.3.2.2. Preparation of (E)-N-(4-chlorobenzylidene)-4-methylbenzenesulfonamide **7***

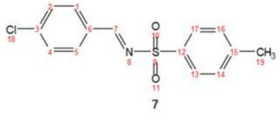

7

According to the general procedure, starting from *p*-chlorobenzaldehyde (0.50 g, 3.56 mmol), *p*-toluenesolfonamide (0.67 g, 3.91 mmol) and Amberlist®-15 in dry toluene (20 mL), compound **7** (0.92 g, 88% yield) was obtained as a white solid.

Data for (*E*)-*N*-(4-chlorobenzylidene)-4-methylbenzenesulfonamide 7: a white solid; ^{1}H NMR (600 MHz, Chloroform-*d*) δ/ppm 2.45 (s, 3H, H-19), 7.36 (d, $J_1 = 8.1$ Hz, 2H, H-14,16), 7.47 (td, $J_1 = 2.3$ Hz, $J_2 = 8.5$ Hz, 2H, H-2,4), 7.84 – 7.92 (m, 4H, H-13,17,5,3), 8.99 (s, 1H, H-7); ^{13}C (75 MHz Chloroform-*d*) δ/ppm 21.7 (C-19), 126.5 (C-6), 128.2 (2C, C-17,13), 129.6 (2C, C-1,5), 129.9 (2C, C-16,14), 132.4 (2C, C-2,4), 134.9 (C-3), 141.5 (C-12) 144.8 (C-15), 168.6 (C-7); IR $\tilde{\nu}_{max}$/cm^{-1}: 3357; 3261; 3064; 1656; 1591; 1558; 1487; 1401; 1315; 1303; 1159; 1082; 820; 786.

Minor signals (marked with *) correspond to residual *p*-toluenesolfonamide ($TsNH_2$) as an impurity.

*3.3.2.3. Preparation of (E)-N-(4-fluorobenzylidene)-4-methylbenzenesulfonamide **8***

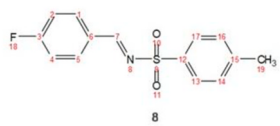

8

According to the general procedure, starting from *p*-fluorobenzaldehyde (0.42 mL, 4.03 mmol), toluene-4-solfonamide (0.76 g, 4.43 mmol) and Amberlist®-15 in dry toluene (20 mL), compound **8** (1.00 g, 89%) was obtained as a white solid.

Data for *(E)-N*-(4-fluorobenzylidene)-4-methylbenzenesulfonamide 8: a white solid; ^{1}H NMR (600 MHz, Chloroform-*d*) δ/ppm 2.44 (s, 3H, H-19), 7.18 (t, $J_1 = 8.5$ Hz, 2H, H-2,4), 7.35 (d, $J_1 = 8.2$ Hz, 2H, H-16,14), 7.88 (d, $J_1 = 8.2$ Hz, 2H, H-13,17), 7.94 – 7.98 (m, 2H, H-1,5), 9.00 (s, 1H, H-7); ^{13}C NMR (151 MHz, Chloroform-*d*) δ/ppm 21.7 (C-19), 116.7 (C-4), 128.1 (2C, C-17,13), 128.8 (C-6), 129.8 (2C, C-1,5), 133.8 (C-14), 135.1 (C-12), 144.7 (C-15), 166.0 ($J_{CF} = 257.5$ Hz, C-3), 168.5 (C-7); IR $\tilde{\nu}_{max}$/cm^{-1}: 3088; 1607; 1595; 1581; 1506; 1412; 1318; 1304; 1231; 1160; 1149; 1086; 807; 768.

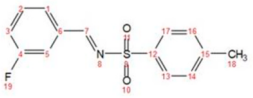

9

*3.3.2.4. Preparation of (E)-N-(3-fluorobenzylidene)-4-methylbenzenesulfonamide **9**.* According to the general procedure, starting from *m*-fluorobenzaldehyde (0.51 mL, 4.83 mmol), toluene-4-solfonamide (0.91 g, 5.32 mmol) and Amberlist®-15 in dry toluene (20 mL), compound **9** (1.1 g, 81% yield) was obtained as white solid.

Data for *(E)-N*-(3-fluorobenzylidene)-4-methylbenzenesulfonamide 9: a white solid; ^{1}H NMR (600 MHz, Chloroform-*d*) δ/ppm 2.45 (s, 3H, H-18), 7.33 – 7.29 (m, 1H, H-3 and $TsNH_2$, overlapped), 7.37 – 7.34 (m, 2H, H-14,16), 7.48 (td, $J_1 = 7.9$ Hz, $J_1 = 5.3$ Hz, 1H, H-2), 7.69 – 7.64 (m, 2H, H-1,5), 7.83 – 7.80 (m, 1H), 7.87 (m, 2H, H-13,17), 7.91 – 9.00 (d, $J_1 = 1.3$ Hz, 1H, H-7); ^{13}C (151 MHz, Chloroform-*d*) δ/ppm 21.7 (C-18), 116.7 ($^{2}J_{CF} = 20.8$ Hz, C-5), 122.0 ($^{2}J_{CF} = 21.6$ Hz, C-3), 126.5 (C-1), 128.2 (2C, C-13,17), 129.9 (2C, C-14,16), 130.9 ($^{3}J_{CF} = 7.8$ Hz, C-2), 134.5 ($^{3}J_{CF} = 7.6$ Hz, C-6), 134.8 (C-12) 144.9 (C-15), 162.9 ($J_{CF} = 249.4$ Hz, CF, C-4), 168.7 (C-7); IR $\tilde{\nu}_{max}$/cm^{-1}: 3357, 3261, 3081, 2919, 1596, 1575, 1452, 1315, 1304, 1157, 1086, 819, 793.

Minor signals (marked with *) correspond to residual *p*-toluenesolfonamide ($TsNH_2$) as an impurity.

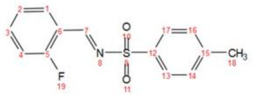

10

*3.3.2.5. Preparation of (E)-N-(2-fluorobenzylidene)-4-methylbenzenesulfonamide **10**.* According to the general procedure, starting from *ortho*-fluorobenzaldehyde (0.36 mL, 3.4 mmol), toluene-4-solfonamide (0.65 g, 3.78 mmol) and Amberlist®-15 in dry toluene (20 mL), compound **10** (0.94 g, 98%) was obtained as a white solid.

Data for *(E)-N*-(2-fluorobenzylidene)-4-methylbenzenesulfonamide 10: a white solid; ^{1}H NMR (300 MHz, Chloroform-*d*) δ/ppm 2.44 (s, 3H, H-18), 7.11 – 7.24 (m, 1H, H-4, 2 and $TsNH_2$, overlapped), 7.36 (d, $J_1 = 8.1$ Hz, 2H, H-16,14), 7.61 (dddd, $J_1 = 8.6$ Hz, $J_2 = 7.3$ Hz, $J_3 = 5.4$ Hz, $J_4 = 1.9$ Hz, 1H, H-3), 7.95 – 7.90 (m, 2H, H-13,17), 8.08 (ddd, $J_1 = 8.3$ Hz, $J_2 = 6.9$ Hz, $J_2 = 1.9$ Hz, 1H, H-1), 9.36 (s, 1H, H-7); ^{13}C (75 MHz, Chloroform-*d*) δ/ppm 21.7 (C-18), 116.4 ($^{2}J_{CF} = 20.5$ Hz, C-4), 120.5 ($^{2}J_{CF} = 8.7$ Hz, C-6), 124.8 ($^{3}J_{CF} = 3.6$ Hz, C-2), 128.2 (2C, C-13,17), 129.4 ($^{4}J_{CF} = 0.8$ Hz, C-1), 129.9 (2C, C-16,14), 134.8 (C-12), 137.0 ($^{3}J_{CF} = 9.2$ Hz, C-3), 144.8 (C-15), 163.6 ($^{3}J_{CF} = 6.2$ Hz, C-7), 164.3 ($J_{CF} = 258.3$ Hz, C-5); IR $\tilde{\nu}_{max}$/cm^{-1}: 3357, 3260, 1605, 1572, 148, 1456, 1320, 1305, 1281, 1087, 830, 761.

Minor signals (marked with *) correspond to residual *p*-toluenesolfonamide ($TsNH_2$) as an impurity.

*3.3.2.6. Preparation of (E)-N-(2,6-difluorobenzylidene)-4-methylbenzenesulfonamide **11***

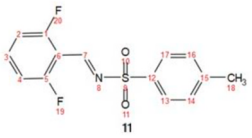

11

According to the general procedure, starting from 2,6-difluorobenzaldehyde (0.56 g, 3.93 mmol), toluene-4-solfonamide (0.74 g, 4.32 mmol) and Amberlist®-15 in dry toluene (20 mL), compound **11** (0.66 g, 57% yield) was obtained as a white solid.

Data for *(E)-N*-(2,6-difluorobenzylidene)-4-methylbenzenesulfonamide 11: a white solid; ^{1}H NMR ($CDCl_3$, 600 MHz) δ/ppm 2.44 (s, 3H, H-18), 7.01 (t, $J_1 = 8.7$ Hz, 2H, H-4,2), 7.35 (d, $J_1 = 8.3$ Hz, 2H, H-14,16), 7.56 (tt, $J_1 = 6.1$ Hz, $J_2 = 8.5$ Hz, 1H, H-3), 7.91 (d, $J_1 = 8.3$ Hz, 2H, H-17,13), 9.31 (s, 1H, H-7); ^{13}C (151 MHz, Chloroform-*d*) δ/ppm 21.7 (C-18), 112.4 ($^{2}J_{CF} = 3.6$ Hz, C-4), 126.5 ($^{2}J_{CF} = 3.8$ Hz, C-2), 128.31 (2C, C-13,17), 129.9 (2C, C-14,16), 134.7 (C-6), 134.7 (C-12), 136.5 ($^{2}J_{CF} = 11.4$ Hz, C-3), 143.7 (C-15), 144.8 ($J_{CF} = 178.5$ Hz, 2C, C-1,5), 160.9 (C-7).

Minor signals (marked with *) correspond to residual *p*-toluenesolfonamide ($TsNH_2$) as an impurity.

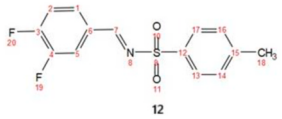

12

*3.3.2.7. Preparation of (E)-N-(3,4-difluorobenzylidene)-4-methylbenzenesulfonamide **12**.* According to the general procedure, starting from 3,4-difluorobenzaldehyde (0.47 mL, 4.22 mmol), toluene-4-solfonamide (0.80 g, 4.64 mmol) and Amberlist®-15 in dry toluene (20 mL), compound **12** (1.0 g, 81%) was obtained as a white solid.

Data for *(E)-N*-(3,4-difluorobenzylidene)-4-methylbenzenesulfonamide 12: a white solid, ^{1}H NMR (600 MHz, Chloroform-*d*) δ/ppm 2.45 (s, 3H, H-18), 7.27 – 7.32 (m, 1H, H-2 and Ts-NH_2, overlapped), 7.36 (d, $J_1 = 8.0$ Hz, 2H, H-16,14), 7.65 – 7.69 (m, 1H, H-5), 7.73 – 7.84 (m, 1H, H-1 and Ts-NH_2, overlapped), 7.86 – 7.90 (m, 2H, H-13,17), 8.96 (d, $J_1 = 1.3$ Hz, 1H, H-7); ^{13}C (151 MHz, Chloroform-*d*) δ/ppm 21.7 (C-18), 118.2 ($^{2}J_{CF} = 18.2$ Hz, C-5), 118.9 ($^{3}J_{CF} = 1.7$ Hz, $^{2}J_{CF} = 18.1$ Hz, C-2), 126.5 (C-1), 128.2 (2C, C-13,17), 129.2 ($^{4}J_{CF} = 5.3$ Hz, $^{3}J_{CF} = 7.7$ Hz, C-6), 129.6 ($^{4}J_{CF} = 3.5$ Hz, $^{3}J_{CF} = 9.4$ Hz, C-5), 129.9 (2C, C-14,16), 134.7 (C-12), 144.97 (C-15), 153.8 ($^{2}J_{CF} = 13.4$ Hz, $J_{CF} = 252.6$ Hz, C-4), 155.3 ($^{2}J_{CF} = 12.9$ Hz, $J_{CF} = 260.7$ Hz, C-3), 167.5 (C-7); IR $\tilde{\nu}_{max}$/cm^{-1}: 3357, 3260, 3059, 1678, 1579, 1520, 1428, 1319, 1300, 1154, 1088, 830, 783.

Minor signals (marked with *) correspond to residual *p*-toluenesolfonamide ($TsNH_2$) as an impurity.

*3.3.2.8. Preparation of (E)-4-methyl-N-(2,4,5-trifluorobenzylidene)benzenesulfonamide **13***

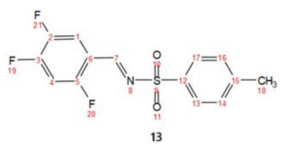

13

According to the general procedure, starting from 2,4,5-

trifluorobenzaldehyde (0.41 mL, 3.75 mmol), toluene-4-solfonamide (0.71 g, 4.12 mmol) and Amberlist®-15 in dry toluene (20 mL), compound **13** (0.90 g, 77%) was obtained as a white solid.

Data for (*E*)-4-methyl-*N*-(2,4,5-trifluorobenzylidene)benzenesulfonamide 13: a white solid; ^{1}H NMR (600 MHz, Chloroform-*d*) δ/ppm 2.45 (s, 3H, H-18), 7.05 (td, $J_1 = 9.4$, 6.1 Hz, 1H, H-4), 7.39 – 7.34 (m, 2H, H-14,16), 7.94 – 7.86 (m, 3H, H-1,13,17), 9.25 (d, $J_1 = 2.2$ Hz, 1H, H-7); ^{13}C (151 MHz, Chloroform-*d*) δ/ppm 21.7 (C-18), 106.5 ($^{2}J_{CF} = 21.3$ Hz, 26.8 Hz, C-4), 116.6 (dt, $^{3}J_{CF} = 2.5$ Hz, $^{2}J_{CF} = 20.3$ Hz, C-1); 117.8 (C-6), 128.3 (2C, C-13,17), 130.0 (2C, C-14,16), 134.4 (C-12), 145.2 (C-15), 147.6 ($^{4}J_{CF} = 3.3$ Hz, $^{3}J_{CF} = 13.2$ Hz, $J_{CF} = 249.8$ Hz, C-5), 155.0 ($^{3}J_{CF} = 12.7$ Hz, $^{2}J_{CF} = 14.9$ Hz, $J_{CF} = 263.9$ Hz, C-2), 160.2 ($^{4}J_{CF} = 1.9$ Hz, $^{3}J_{CF} = 10.3$ Hz, $J_{CF} = 259.5$ Hz, C-3), 161.5 ($^{3}J_{CF} = 5.1$ Hz, C-7); IR $\tilde{\nu}_{max}$/cm^{-1}: 3357, 3261, 3071, 1613, 1594, 1506, 1438, 1338, 1322, 1296, 1154, 1087, 888, 786.

Note: This imine intermediate was successfully synthesized and fully characterized, the corresponding final product was not included in the present study.

3.3.3. Preparation of halogenated quinolinone-aziridines (±)-*14*–*20*

General procedure for preparation of halogenated quinolinone-aziridines (±)-**14**–**20:** To a flame dried Schlenk flask was added quinoline-2(1*H*)-on salt **6** (1 equiv.), which was stirred under vacuum for 0.5 h, and then suspended in dry CH_3CN under an atmosphere of argon. Potassium hydroxide (2 equiv.) was added and the resulting orange solution was stirred 0.5 h at room temperature before addition of the corresponding *N*-Ts-aldimines **6**–**13** (1 equiv.). After the addition was complete, the resulting suspension was stirred overnight. The reaction was quenched by the addition of water (10 mL). The aqueous solution was extracted with ethyl acetate (3 x 20 mL). The combined organic layers were washed with brine (20 mL), dried over anhydrous Na_2SO_4 and filtered. The solvent was removed in *vacuo* to give a solid. The crude product was purified *via* column chromatography (*flash* silica gel, dichloromethane/methanol = 25/1), and recrystallized from methanol/dichloromethane (9/1) to give products (±)-**14**–**20** as a pale yellow or white solid.

3.3.3.1. Preparation of 1-methyl-3-phenyl-1-tosylaziridin-2-yl)quinolin-2(1H)-one (±)-*14*

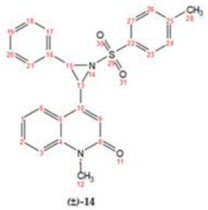

According to the general procedure, starting from *N*-Ts-aldimine **6** (0.19 g, 0.46 mmol), **5** (0.18 g, 0.46 mmol) and KOH (0.05 g, 0.91 mmol) in dry CH_3CN (15 mL), the reaction afforded a crude mixture containing the desired product along with residual starting material (imine, salt) and byproducts. The crude ^{1}H NMR indicated a d.r. (*cis*:*trans)* ratio of 14:86 (Fig. S21). Purification by column chromatography and recrystallization from MeOH/DCM (9/1) afforded (±)-*trans*-**14** as a pure compound (80 mg, 39% yield), while the minor *cis* diastereomer remained in fractions containing mixtures with the *trans* isomer (70 mg, 33% yield).

Data for 1-methyl-3-phenyl-1-tosylaziridin-2-yl)quinolin-2(1*H*)-one (±)**-14:** Major diastereomer (±)-*trans*-**14**: a white solid; m.p. 90.0 – 91.1 °C; ^{1}H NMR (600 MHz, Chloroform-*d*) δ/ppm 2.41 (s, 3H, H-28), 3.70 (s, 3H, H-12), 4.06 (d, $J_1 = 4.6$ Hz, 1H, H-15), 4.60 (dd, $J_1 = 0.6$ Hz, $J_2 = 4.6$ Hz, 1H, H-13), 6.67 (d, $J_1 = 0.6$ Hz, 1H, H-9), 7.22 – 7.30 (m, 3H, H-3,21,17), 7.39 – 7.47 (m, 4H, H-19,1,26,18), 7.52 – 7.57 (m, 2H, H-24,20), 7.62 (s, 1H, H-2), 7.65 – 7.69 (m, 1H, H-23,27), 7.90 (dd, $J_1 = 1.6$ Hz, $J_2 = 8.0$ Hz, 1H, H-6); ^{13}C NMR (75 MHz, Chloroform-*d*) δ/ppm 21.65 (C-28), 29.47 (C-12), 45.68 (C-13), 50.61 (C-15), 114.65 (C-3), 119.75 (C-5), 120.21 (C-9), 122.34 (C-1), 125.03 (C-6), 127.73 (2C, C-17,21), 128.64 (2C, C-18,20), 128.62 (2C, C-24,26), 129.23 (C-19), 129.62 (C-2), 131.08 (C-16), 131.43 (C-16), 136.34 (C-22), 139.91 (C-4) 142.28 (C-25), 144.65 (C-10), 161.63 (C-8); IR $\tilde{\nu}_{max}$/cm^{-1}: 3062, 1649, 1591, 1499, 1455, 1321, 1158, 1087, 911, 812, 750, 687; HRMS 453.12602 (calculated for $C_{25}H_{22}N_2O_3S$ $[M+Na]^+$ 453.12488).

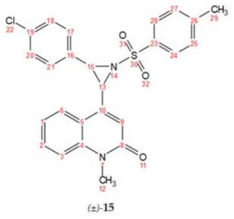

3.3.3.2. Preparation of 3-(4-chlorophenyl)-1-tosylaziridin-2-yl)-1-methylquinolin-2(1H)-one (±)-*15*

According to the general procedure, starting from *N*-Ts-aldimine **7** (0.13 g, 0.46 mmol), **5** (0.18 g, 0.46 mmol) and KOH (0.05 g, 0.91 mmol) in dry CH_3CN (15 mL), the reaction afforded a crude mixture containing the desired product along with residual starting material (imine, salt) and byproducts. The crude ^{1}H NMR indicated a d.r. (*cis*:*trans*) ratio of 20:80 (Fig. S22). Purification by column chromatography enabled partial separation, affording (±)-*trans*-**15** (55 mg, 25% yield) and (±)-*cis*-**15** (15 mg, 7% yield), along with additional fractions containing mixtures of both diastereomers (110 mg, 49% yield).

Data for 3-(4-chlorophenyl)-1-tosylaziridin-2-yl)-1-methylquinolin-2(1*H*)-one (±)**-15:** Major diostereomer (±)-*trans*-**15**: a white solid; m.p. = 216.3 – 217.5 °C; ^{1}H NMR (600 MHz, Chloroform-*d*) δ/ppm 2.41 (s, 3H, H-29), 3.69 (s, 3H, H-12), 4.02 (d, $J_1 = 4.6$ Hz, 1H, H-15), 4.54 (d, $J_1 = 4.6$ Hz, 1H, H-13), 6.65 (s, 1H, H-9), 7.19 – 7.26 (m, 2H, H-3,21), 7.26 – 7.32 (m, 2H, H-17,25), 7.36 – 7.43 (m, 3H, H-27,1,18), 7.57 – 7.70 (m, 3H, H-20,2,6), 7.82 (t, $J_1 = 8.3$ Hz, 2H, H-24,28); ^{13}C NMR (151 MHz, Chloroform-*d*) δ/ppm 21.8 (C-29), 29.4 (C-12), 45.3 (C-13), 46.2 (C-15), 114.8 (C-3), 118.9 (C-9), 121.2 (C-1), 122.3 (C-5), 124.0 (C-6), 128.0 (2C, C-18,20), 128.5 (2C, C-25,27), 128.6 (2C, C-17,21), 129.6.0 (C-2), 130.1 (2C, C-28,24), 131.00 (C-19), 134.2 (C-16), 134.4 (C-23), 139.6 (C-26), 139.7 (C-4), 145.5 (C-10), 161.3 (C-8); IR $\tilde{\nu}_{max}$/cm^{-1}: 3050, 1655, 1590, 1493, 1456, 1375, 1319, 1158, 1087, 914, 810, 753, 679; HRMS 465.10437 (calculated for $C_{25}H_{21}ClN_2O_3S$ $[M+H]^+$ 465.10397).

Minor diostereomer (±)-*cis*-**15**: a white solid; m.p. = 223.4 – 224.7 °C; ^{1}H NMR (600 MHz, Chloroform-*d*) δ/ppm 2.48 (s, 3H, H-29); 3.61 (s, 3H, H-12), 4.39 (dd, $J_1 = 7.3$ Hz, $J_2 = 1.2$ Hz, 1H, H-15), 4.48 (d, $J_1 = 7.3$ Hz, 1H, H-13), 6.60 (d, $J_1 = 1.2$ Hz, 1H, H-9), 7.13 – 7.04 (m, 4H, H-17,21,25,27), 7.25 (ddd, $J_1 = 8.2$ Hz, $J_2 = 7.3$ Hz, $J_3 = 1.0$ Hz, 1H, H-3), 7.32 – 7.27 (m, 1H, H-1), 7.42 – 7.38 (m, 2H, H-18,20), 7.55 (ddd, $J_1 = 8.6$ Hz, $J_2 = 7.2$ Hz, $J_3 = 1.5$ Hz, 1H, H-2), 7.77 (dd, $J_1 = 8.0$, $J_2 = 1.5$ Hz, 1H, H-6), 8.00 – 7.94 (m, 2H, H-24,28), ^{13}C NMR (151 MHz, Chloroform-*d*) δ/ppm 161.32 (C-8), 145.51 (C-10), 139,69 (C-26), 139.51 (C-4),134.36 (C-23), 134.20 (C-16), 130.97 (C-2), 130.14 (C-18,20), 129.62 (C-19), 128.58 (C-25,27), 128.46 (C-17,21), 128.03 (C-24,28), 123.96 (C-6), 122.24 (C-1), 121.26 (C-9), 118.93 (C-5), 114.77 (C-3), 46.16 (C-15), 45.36 (C-13), 29.34 (C-12), 21.77 (C-29); IR $\tilde{\nu}_{max}$/cm^{-1}: 3050, 1655, 1590, 1493, 1456, 1375, 1319, 1158, 1087, 914, 810, 753, 679; HRMS 465.10437 (calculated for $C_{25}H_{21}ClN_2O_3S$ $[M+H]^+$ 465.10397).

3.3.3.3. Preparation of 3-(4-fluorophenyl)-1-tosylaziridin-2-yl)-1-methylquinolin-2(1H)-one (±)-*16*

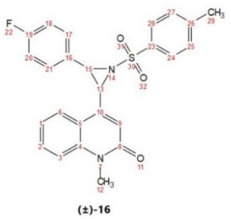

(±)-16

According to the general procedure, starting from *N*-Ts-aldimine **8** (0.04 g, 0.13 mmol), **5** (0.05 g, 0.13 mmol) and KOH (0.01 g, 0.26 mmol) in dry CH_3CN (15 mL), the reaction afforded a crude mixture containing the desired product along with residual starting material (imine, salt) and byproducts. The crude ^{1}H NMR showed a d.r. (*cis*:*trans)* ratio of 18:82 (Fig. S23). Purification by column chromatography enabled partial separation, affording (±)-*trans*-**16** (37 mg, 62% yield) and (±)-*cis*-**16** (8 mg, 14% yield).

Data for 3-(4-fluorophenyl)-1-tosylaziridin-2-yl)-1-methylquinolin-2(1*H*)-one (±)-**16:** Major diastereomer (±)-*trans*-**16**: a white solid; m.p. 99.6 – 101.8 °C; ^{1}H NMR (600 MHz, Chloroform-*d*) δ/ppm 2.44 (s, 3H, H-29), 3.72 (s, 3H, H-12), 4.02 (d, $J_1 = 4.6$ Hz, 1H, H-15), 4.61 (dd, $J_1 = 4.7$, $J_2 = 1.1$ Hz, 1H, H-13), 6.64 (d, $J_1 = 1.1$ Hz, 1H, H-9), 7.17 – 7.10 (m, 2H, H-20,18), 7.31 – 7.24 (m, 3H, H-1,25,27), 7.44 – 7.40 (m, 1H, H-3), 7.57 – 7.52 (m, 2H, H-17,21), 7.63 (ddd, $J_1 = 8.6$ Hz, $J_2 = 7.2$ Hz, $J_3 = 1.5$ Hz, 1H, H-2), 7.71 – 7.66 (m, 2H, H-24,28), 7.86 (dd, $J_1 = 8.0$ Hz, $J_2 = 1.4$ Hz, 1H, H-6); ^{13}C NMR (151 MHz, Chloroform-*d*) δ/ppm 21.66 (C-29), 29.49 (C-12), 45.60 (C-15), 50.18 (C-13), 114.71 (C-3), 115.73 (C-20), 115.76 (C-18), 119.64 (C-5), 120.10 (C-9), 122.36 (C-1), 124.84 (C-6), 127.15 (C-16), 127.69 (2C, C-28,24)), 129.61 (2C, C-21,17), 130.77 C-25); 130.82 (C-27), 131.13 (C-2), 136.30 (C-23), 139.94 (C-4), 142.28 (C-26), 144.80 (C-10), 161.58 (C-8); IR $\tilde{\nu}_{max}$/cm^{-1}: 3065, 1652, 1592, 1513, 1456, 1371, 1322, 1158, 1087, 940, 814, 751, 685; HRMS 449.13412 (calculated for $C_{25}H_{21}FN_2O_3S$ $[M+H]^+$ 449.13352).

Minor diostereomer (±)-*cis*-**16:** a white solid; 110.4 – 111.9 °C; ^{1}H NMR (600 MHz, Chloroform-*d*) δ/ppm 7.90 – 7.87 (m, 2H, H-24,28), 7.69 (dd, $J_1 = 8.0$ Hz, $J_2 = 1.5$ Hz, 1H, H-6), 7.46 (ddd, $J_1 = 8.7$ Hz, $J_2 = 7.2$ Hz, $J_3 = 1.5$ Hz, 1H, H-2), 7.31 (dq, $J_1 = 7.0$ Hz, $J_2 = 1.2$ Hz, $J_3 = 0.8$ Hz, 2H, H-17,21), 7.21 – 7.19 (m, 1H, H-27), 7.16 (ddd, $J_1 = 8.1$ Hz, $J_2 = 7.2$ Hz, $J_3 = 1.1$ Hz, 1H, H-25), 7.04–7.00 (m, 2H, H-1,3), 6.71 – 6.67 (m, 2H, H-18,20), 6.50 (d, $J_1 = 1.2$ Hz, 1H, H-9), 4.40 (d, $J_1 = 7.3$ Hz, 1H, H-13), 4.29 (dd, $J_1 = 7.3$ Hz, $J_2 = 1.2$ Hz, 1H, H-15), 3.51 (s, 3H, H-12), 2.39 (s, 3H, H-29); ^{13}C NMR (151 MHz, Chloroform-*d*) δ/ppm 161.70 (C-19, $J_{CF} = 248.3$ Hz), 161.34 (C-8), 145.46 (C-10), 139.66 (C-26), 134.42 (C-4), 130.93 (C-23), 130.13 (C-17,21), 128.99 (C-25,27), 128.03 (C-24,28), 126.83 (C-16, $J_{CF} = 3.11$ Hz), 124.01 (C-2,6), 122.22 (C-1), 121.26 (C-9), 118.97 (C-5), 115.35 (C-18), 115.21 (C-20), 114.72 (C-3), 46.16 (C-15), 45.35 (C-13), 29.33 (C-12), 21.76 (C-29); IR $\tilde{\nu}_{max}$/cm^{-1}: 3065, 1652, 1592, 1513, 1456, 1371, 1322, 1158, 1087, 940, 814, 751, 685; HRMS 449.13412 (calculated for $C_{25}H_{21}FN_2O_3S$ $[M+H]^+$ 449.13352).

*3.3.3.4. Preparation of 3-(3-fluorophenyl)-1-tosylaziridin-2-yl)-1-methylquinolin-2(1H)-one (±)-cis-**17***

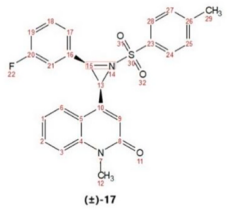

(±)-17

According to the general procedure, starting from *N*-Ts-aldimine **9** (0.11 g, 0.39 mmol), **5** (0.15 g, 0.39 mmol) and KOH (0.04 g, 0.78 mmol) in dry CH_3CN (15 mL), compound (±)-*cis*-**17** was obtained as a white solid (0.09 g, 51% yield). The crude ^{1}H NMR indicated a d.r. (*cis*:*trans*) ratio of 100:0 (Fig. S24), indicating complete diastereoselectivity.

Data for 3-(3-fluorophenyl)-1-tosylaziridin-2-yl)-1-methylquinolin-2(1*H*)-one (±)-*cis*-**17**: a white solid; m.p. 215.5 – 216.9 °C; ^{1}H NMR (600 MHz, Chloroform-*d*) δ/ppm 2.45 (s, 3H, H-29), 3.55 (s, 3H, H-12), 4.39 (dd, $J_1 = 1.1$ Hz, $J_2 = 7.4$ Hz, 1H, H-15), 4.48 (d, $J_1 = 7.3$ Hz, 1H, H-13), 6.59 (d, $J_1 = 1.2$ Hz, 1H, H-9), 6.75 (tdd, $J_1 = 1.0$ Hz, $J_2 = 2.6$ Hz, $J_3 = 8.5$ Hz, 1H, H-19), 6.82 (dt, $J_1 = 2.2$ Hz, $J_2 = 9.5$ Hz, 1H, H-21), 6.92 (ddt, $J_1 = 0.8$, $J_2 = 1.6$ Hz, $J_3 = 7.8$ Hz, H-3), 7.03 (td, $J_1 = 5.7$ Hz, $J_2 = 8.0$ Hz, 1H, H-17), 7.23 (td, $J_1 = 1.2$ Hz, $J_2 = 7.6$ Hz, $J_3 = 8.1$ Hz, 2H, H-18,25), 7.34 – 7.42 (m, 2H, H-1,27), 7.51 (ddd, $J_1 = 1.5$ Hz, $J_1 = 7.3$ Hz, $J_3 = 8.7$ Hz, H-2), 7.73 – 7.80 (m, 1H, H-6), 7.92 – 8.00 (m, H-24,26); ^{13}C (151 MHz, Chloroform-*d*) δ/ppm 21.7 (C-29), 29.3 (C-12), 45.3 (C-13), 46.2 ($^4J_{CF} = 2.3$ Hz, C-15), 114.3 ($^2J_{CF} = 22.9$ Hz, C-21), 114.7 (C-3), 115.4 ($^2J_{CF} = 21.2$ Hz, C-19), 118.9 (C-9), 121.2 (C-1), 122.3 (C-17), 123.1 ($^4J_{CF} = 2.8$ Hz, C-5), 124.0 (C-6), 128.1 (2C, C-24,28), 129.8 ($^3J_{CF} = 8.3$ Hz, C-18), 130.2 (2C, C-27,25), 131.0 (C-2), 133.6 ($^3J_{CF} = 7.8$ Hz, C-16), 134.3 (C-23), 139.5 (C-4), 139.6 (C-26), 145.5 (C-10), 161.3 (C-8), 163.1 ($J_{CF} = 247.1$ Hz, C-20); IR $\tilde{\nu}_{max}$/cm^{-1}: 3034, 1656, 1591, 1491, 1451, 1322, 1155, 1088, 954, 869, 749, 675; HRMS 449.13452 (calculated for $C_{25}H_{21}FN_2O_3S$ $[M+H]^+$ 449.1335).

*3.3.3.5. Preparation of 3-(2-fluorophenyl)-1-tosylaziridin-2-yl)-1-methylquinolin-2(1H)-one (±)-**18***

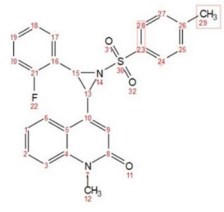

(±)-18

According to the general procedure, starting from *N*-Ts-aldimine **10** (0.11 g, 0.39 mmol), **5** (0.15 g, 0.39 mmol) and KOH (0.04 g, 0.78 mmol) in dry CH_3CN (15 mL), the reaction afforded a crude mixture containing the desired product along with residual starting material (imine, salt) and byproducts. The crude ^{1}H NMR showed a d.r. (*cis/trans*) ratio of 21:79 (Fig. S25). Purification by column chromatography enabled partial separation, affording (±)-*trans*-**18** (59 mg, 33% yield) and (±)-*cis*-**18** (14 mg, 8%), along with additional fractions containing mixtures of both diastereomers (57 mg, 32%).

Data for 3-(2-fluorophenyl)-1-tosylaziridin-2-yl)-1-methylquinolin-2(1*H*)-one (±)-**18:** Major diastereomer (±)-*trans*-**18**: a white solid; m.p. 97.3 – 98.5 °C; ^{1}H NMR (600 MHz, Chloroform-*d*) δ/ppm 7.96 (dd, $J_1 = 8.0$, $J_2 = 1.4$ Hz, 1H, H-6), 7.71 – 7.65 (m, 2H, H-24,28), 7.63 (td, $J_1 = 8.3$ Hz, $J_2 = 7.8$ Hz, $J_3 = 1.4$ Hz, 1H, H-2), 7.55 (td, $J_1 = 7.7$ Hz, $J_2 = 1.5$ Hz, 1H, H-1), 7.41 (dd, $J_1 = 8.8$, $J_2 = 5.8$ Hz, 2H, H-25,27), 7.30–7.24 (m, 4H, H-1,3,17,19), 7.14 (ddd, $J_1 = 10.5$, $J_2 = 8.3$ Hz, $J_3 = 1.2$ Hz, 1H, H-20), 6.71 (d, $J_1 = 1.1$ Hz, 1H, H-9), 4.65 (d, $J_1 = 4.7$ Hz, 1H, H-13), 4.16 (d, $J_1 = 4.6$ Hz, 1H, H-15), 3.72 (s, 3H, H-12), 2.43 (s, 3H, H-29); ^{13}C NMR (151 MHz, Chloroform-*d*) δ 161.59 (C-8), 161.34 (C-21, $J_{CF} = 250.0$ Hz), 144.85 (C-10), 142.17 (C-26), 139.92 (C-4), 135.86 (C-23), 131.09 (C-18,19, $J_{CF} = 2.15$ Hz), 131.02 (C-2), 129.85 (C-17, $J_{CF} = 2.83$ Hz), 129.64 (2C, C-25,27), 127.85 (2C, C-24,28), 125.05 (C-6), 124.25 (C-16, $J_{CF} = 3.63$ Hz), 122.34 (C-1), 120.33 (C-9), 119.72 (C-5), 115.69 (C-20, $J_{CF} = 21.4$ Hz), 114.62 (C-3), 45.00 (C-15), 44.89 (C-13), 29.48 (C-12), 21.67 (C-29); IR $\tilde{\nu}_{max}$/cm^{-1}: 3355, 3260, 3065, 2923, 1646, 1588, 1495, 1455, 1328, 1305, 1157, 1086, 915, 813, 753, 687; HRMS 449.13472 (calculated $C_{25}H_{21}FN_2O_3S$

$[M+H]^+$ 449.13352).

Minor diastereomer (±)-*cis*-**18:** a white solid; m.p. 94.2 – 95.7 °C, ^{1}H NMR (600 MHz, Chloroform-*d*) δ/ppm 8.00 – 7.95 (m, 2H, H-24,28), 7.77 (dd, $J_1 = 8.0$ Hz, $J_2 = 1.5$ Hz, 1H, H-6), 7.54 (ddd, $J_1 = 8.6$ Hz, $J_2 = 7.2$, $J_3 = 1.5$ Hz, 1H, H-2), 7.42 – 7.37 (m, 2H, H-25,27), 7.28 (dd, $J_1 = 8.6$ Hz, $J_2 = 1.0$ Hz, 1H, H-1), 7.25 (ddd, $J_1 = 8.1$ Hz, $J_2 = 7.2$ Hz, $J_3 = 1.0$ Hz, 1H, H-3), 7.14 – 7.08 (m, 2H, H-17,19), 6.80–6.74 (m, 2H, H-18,20), 6.59 (d, $J_1 = 1.2$ Hz, 1H, H-9), 4.49 (d, $J_1 = 7.3$ Hz, 1H, H-13), 4.38 (dd, $J_1 = 7.3$, $J_2 = 1.2$ Hz, 1H, H-15), 3.59 (s, 3H, H-12), 2.47 (s, 3H, H-29); ^{13}C NMR (151 MHz, Chloroform-*d*) δ/ppm 161.68 ($J_{CF} = 248.8$ Hz, C-21), 161.33 (C-8), 145.46 (C-10), 139.65 ($^3J_{CF} = 3.1$ Hz, C-17,19), 134.42 (C-4), 130.94 (C-23), 130.13 (C-25,27), 128.95 ($^2J_{CF} = 8.3$ Hz, C-16), 128.03 (C-24,28), 126.85 ($^4J_{CF} = 3.1$ Hz, C-18), 124.02 (C-6), 122.22 (C-5), 121.25 (C-1), 118.96 (C-9), 115.28 ($^2J_{CF} = 22.1$ Hz, C-20), 114.72 (C-3), 46.17 (C-13), 45.35 (C-15), 29.32 (C-12), 21.76 (C-29); IR $\tilde{\nu}_{max}$/cm^{-1}: 3355, 3260, 3065, 2923, 1646, 1588, 1495, 1455, 1328, 1305, 1157, 1086, 915, 813, 753, 687; HRMS 449.13472 (calculated $C_{25}H_{21}FN_2O_3S$ $[M+H]^+$ 449.13352).

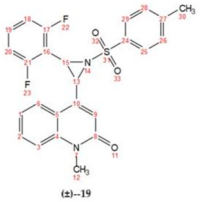

(±)-19

*3.3.3.6. Preparation of 3-(2,6-difluorophenyl)-1-tosylaziridin-2-yl)-1-methylquinolin-2(1H)-one (±)-trans-**19**.* According to the general procedure, starting from *N*-Ts-aldimine **11** (0.12 g, 0.31 mmol), **5** (0.10 g, 0.26 mmol) and KOH (0.03 g, 0.52 mmol) in dry CH_3CN (15 mL), compound (±)-*trans*-**19** was obtained as a white solid (90 mg, 74% yield). The crude ^{1}H NMR showed d.r. (*cis*:*trans*) ratio of 0:100 (Fig. S26), indicating complete diastereoselectivity.

Data of 3-(2,6-difluorophenyl)-1-tosylaziridin-2-yl)-1-methylquinolin-2(1*H*)-one (±)-*trans*-**19:** a white solid; m.p. 91.2 – 92.0 °C; ^{1}H NMR (600 MHz, Chloroform-*d*) δ/ppm: 2.43 (s, 3H, H-30), 3.69 (s, 3H, H-12), 3.78 (d, $J_1 = 4.6$ Hz, 1H, H-15), 5.15 (d, $J_1 = 4.8$ Hz, 1H, H-13), 6.64 (s, 1H, H-9), 7.00 (t, $J_1 = 8.5$ Hz, 2H, H-18,20), 7.25 – 7.36 (m, 3H, H-3,1,19), 7.37 – 7.44 (m, 2H, H-26,28), 7.62 (t, $J_1 = 7.4$ Hz, 1H, H-2), 7.76 (d, $J_1 = 8.3$ Hz, 2H, H-25,29), 8.11 (d, $J_1 = 8.0$ Hz, 1H, H-6); ^{13}C NMR (151 MHz, Chloroform-*d*) δ/ppm: 21.7 (C-30), 29.5 (C-12), 42.7 (C-13), 43.0 (C-15), 111.73 ($^2J_{CF} = 3.5$ Hz, C-20), 111.87 ($^2J_{CF} = 3.5$ Hz, C-18), 114.68 (C-3), 119.11 (C-9), 119.48 (C-1), 122.50 (C-6), 124.69 ($^3J_{CF} = 3.2$ Hz, C-16), 126.44 (C-4,5), 127.89 (2C, C-25,29), 129.74 (2C, C-26,28), 131.11 (C-24), 132.20 ($^4J = 1.5$ Hz, C-19); 135.73 (C-27), 139.92 (C-4), 143.50 (C-10), 145.00 (C-17,21, $J_{CF} = 246.5$ Hz), 161.8 (C-8), IR $\tilde{\nu}_{max}$/cm^{-1}: 3067; 1648; 1590; 1469; 1455; 1372; 1325; 1160; 1084; 995; 938; 682; HRMS 468.12759 (calculated for $C_{25}H_{20}F_2N_2O_3S$ $[M+H]^+$467.12410).

*3.3.3.7. Preparation of 3-(3,4-difluorophenyl)-1-tosylaziridin-2-yl)-1-methylquinolin-2(1H)-one (±)-**20***

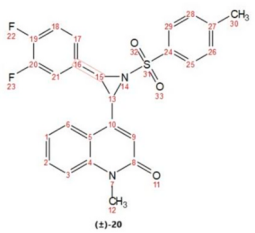

(±)-20

According to the general procedure, starting from *N*-Ts-aldimine **12** (0.12 g, 0.39 mmol), **5** (0.15 g, 0.39 mmol) and KOH (0.04 g, 0.78 mmol) in dry CH_3CN (15 mL), the reaction afforded a crude mixture containing the desired product along with residual starting material (imine, salt) and byproducts. The crude ^{1}H NMR showed a d.r. (*cis*:*trans)* ratio of 14:86 (Fig. S27). Purification by column chromatography afforded (±)-*trans*-**20** as a pure compound (45 mg, 24% yield), and (±)-*cis*-**20** (11 mg, 6%), along with additional fractions containing mixtures of both diastereomers (45 mg, 32%).

Data for 3-(3,4-difluorophenyl)-1-tosylaziridin-2-yl)-1-methylquinolin-2(1H)-one (±)-**20** Major diastereomer (±)-*trans*-**20:** a white solid; m.p. 217.1 – 218.8 °C; ^{1}H NMR (600 MHz, Chloroform-*d*) δ/ppm: 2.42 (s, 3H, H-30), 3.70 (s, 3H, H-12), 4.04 (d, $J_1 = 4.7$ Hz, 1H, H-15), 4.47 (d, $J_1 = 4.7$ Hz, 1H, H-13), 6.65 (s, 1H, H-9), 7.15 – 7.40 (m, 6H, H-1,2,3,17,18,21), 7.57 – 7.71 (m, 3H, H-6,25,29), 7.75 – 7.88 (m, 2H, H-26,28); ^{13}C (151 MHz, Chloroform-*d*) δ/ppm: 21.65 (C-30), 29.51 (C-12), 46.53 (C-13), 48.67 (C-15), 114.74 (C-3), 117.75 ($^3J_{CF} = 4.3$ Hz, $^2J_{CF} = 6.4$ Hz, C-18,21), 119.66 (C-3), 120.39 (C-9), 122.42 (C-1), 124.93 (C-5), 125.09 ($^3J = 5.1$ Hz, C-17), 126.43 (C-6), 127.73 (2C, C-25,29), 128.84 ($^3J_{CF} = 4.9$ Hz, C-16), 129.72 (2C, C-26,28), 131.21 (C-2), 136.01 (C-24), 139.89 (C-4), 141.67 (C-27), 145.02 (C-10), 148.91 ($^2J_{CF} = 14.1$ Hz, $J_{CF} = 39.7$ Hz, C-19), 152.28 ($^2J_{CF} = 14.3$ Hz, $J_{CF} = 41.1$ Hz, C-20), 161.53 (C-8); IR $\tilde{\nu}_{max}$/cm^{-1}: 3043, 1654, 1590, 1518, 1455, 1317, 1203, 1159, 1086, 938, 898, 753, 686; HRMS 467.12482 (calculated for $C_{25}H_{20}F_2N_2O_3S$ $[M+H]^+$ 467.12410).

Major diastereomer (±)-*cis*-**20:** a white solid; m.p. 201.5 – 202.9 °C; ^{1}H NMR (600 MHz, Chloroform-*d*) δ/ppm: 2.48 (s, 3H, H-30); 3.61 (s, 3H, H-12), 4.37 (dd, $J = 7.3$, 1.2 Hz, 1H, H-15), 4.44 (d, $J = 7.3$ Hz, 1H, H-13), 6.56 (d, $J = 1.2$ Hz, 1H, H-9), 6.90 – 6.87 (m, 2H, H-18,21), 6.97 – 6.91 (m, 1H, H-3), 7.26 – 7.24 (m, 1H, H-17), 7.30 (d, $J = 8.5$ Hz, 1H, H-1), 7.42 – 7.39 (m, 2H, H-26,28), 7.56 (ddd, $J = 8.6$, 7.2, 1.5 Hz, 1H, H-2), 7.75 (dd, $J = 8.0$, 1.5 Hz, 1H, H-6), 7.98 – 7.94 (m, 2H, H-25,29); ^{13}C (151 MHz, Chloroform-*d*) δ/ppm: 21.78 (C-30); 29.36 (C-12); 45.41 (C-13); 45.49 (C-15); 114.82 (C-3); 116.41 ($^2J_{CF} = 18.9$ Hz, C-18,21); 117.27 ($^2J_{CF} = 18.9$ Hz, C-17); 121.27 (C-5); 122.31 (C-9); 123.46 (C-1); 123.88 (C-6); 128.06 (C-25,29); 130.20 (C-26,28); 131.08 (C-2); 118.83 (C-5); 128.02 (C-16); 130.18 (C-24); 134.20 (C-4); 139.34 (C-27); 139.72 (C-10); 145.67 (C-19) 149.44 (C-20); 161.25 (C-8); IR $\tilde{\nu}_{max}$/cm^{-1}: 3043, 1654, 1590, 1518, 1455, 1317, 1203, 1159, 1086, 938, 898, 753, 686; HRMS 467.12482 (calculated for $C_{25}H_{20}F_2N_2O_3S$ $[M+H]^+$ 467.12410).

*Due to low intensity of the ^{13}C NMR signals, the corresponding coupling constants ($J_{C\text{-}F,}$ C-19,20) could not be determined reliably.

3.4. HPLC analysis

HPLC analysis was performed using an Agilent 1260 Infinity II equipped with a diode array detector (DAD) and a Synergi 4 µm Polar-RP 80A, 4.6 × 150 mm, Phenomenex) column. The mobile phase consisted of water containing 0.1% phosphoric acid (A) and acetonitrile (B), using gradient of 5–100% B over 30 min. The flow rate was 0.5 mL/min, and detection was carried out over a wavelength range of 200–400 nm, with chromatograms monitored at 210 and 254 nm. All compounds were obtained with a purity ≥98% as determined by HPLC.

3.5. Biological activity

3.5.1. Antiproliferative activity

3.5.1.1. Cell lines. Biological evaluation was performed on a panel of three human cell lines: H460 (non-small cell lung carcinoma), MCF-7 (breast adenocarcinoma), and HEK293T (hu-man embryonic kidney).

3.5.1.2. Cell culture conditions. Cells were grown as adherent monolayers in Dulbecco's Modified Eagle Medium (DMEM) supplemented with 10% fetal bovine serum (FBS), 2 mM L-glutamine, 100 U/mL

penicillin, and 100 μg/mL streptomycin. Cultures were maintained in a humidi-fied incubator at 37 °C under 5% CO_2 atmosphere.

3.5.1.3. Cell proliferation assay (MTT). Cells were seeded in 96-well plates at a density of 1.5×10^4 cells/mL (or 2×10^4 cells/mL for MCF-7), adjusted according to the specific doubling time of each cell line. Test compounds were added in a series of five 10-fold serial dilutions (10^{-8} to 10^{-4} M), and cells were incubated for 72 h. Stock solutions were freshly prepared on the day of testing, and the final concentration of solvent did not exceed 0.5%.

After incubation, cell viability was assessed using the MTT assay [37], which measures mitochondrial dehydrogenase activity in metabolically active cells. The culture medium was removed, and 40 μL of MTT reagent (0.5 μg/μL) was added to each well. Following a 4-h incubation, the formazan crystals formed were solubilized with 160 μL of DMSO. Absorbance was measured at 570 nm using a microplate reader, and cell viability was expressed as a percentage relative to the untreated control. The percentage of growth (PG) was calculated according to standard formulas:

If $(A_{test} - At_{zero}) \geq 0$ then:

$$PG = 100 \times (A_{test} - A_{tzero}) / (A_{cont} - A_{tzero})$$

If $(A_{test} - A_{tzero}) < 0$ then:

$$PG = 100 \times (A_{test} - A_{tzero}) / A_{tzero}$$

Where:

A_{tzero} = the average absorbance before exposure of cells to the test compound.

A_{test} = the average absorbance after the desired period of time (72 h)

A_{cont} = the average absorbance after 72 h with no exposure of cells to the test compound.

Each test point was performed in quadruplicate across three independent experiments. Negative percentages indicate cytotoxicity, with a value of −100% signifying total cell death at a given compound concentration. Growth inhibition values (GI_{50}), representing the concentration required to inhibit cell proliferation by 50%, were determined from the dose–response curves (Table S3).

GI_{50} values were calculated *via* linear regression by interpolating between data points flanking the 50% growth threshold. If none of the tested concentrations fell below the reference threshold (e.g., PG < 50), the lowest tested concentration was reported as a default and marked with a "<" symbol. Conversely, if all tested concentrations resulted in growth below the threshold, the highest concentration was reported with a ">" symbol. These notations indicate that the actual GI_{50} value lies outside the tested concentration range.

3.5.2. Zebrafish embryotoxicity assay

A zebrafish embryotoxicity test (ZET) was performed in accordance with OECD 236 (2013) [38] For dose range-finding experiments, embryos ($N = 10$ per concentration) were exposed to serial dilutions across a broad concentration range: (±)-*trans*-**14** (0.026 - 0.0008125 mg/mL), (±)-*trans*-**15** (0.026 - 0.0008125 mg/mL), (±)-*trans*-**16** (0.02 - 0.000625 mg/mL), (±)-*trans*-**18** (0.038 - 0.0011875 mg/mL), (±)-*trans*-**19** (0.02 - 0.000625 mg/mL), (±)-*trans*-**20** (0.04 - 0.00125 mg/mL), (±)-*cis*-**15** (0.02 – 0.000625 mg/mL), (±)-*cis*-**16** (0.032 - 0.001 mg/mL), (±)-*cis*-**17** (0.03 - 0.0009375 mg/mL), (±)-*cis*-**18** (0.026 - 0.0008125 mg/mL), (±)-*cis*-**20** (0.02 - 0.000625 mg/mL). The highest tested concentration for each compound was selected based on the maximum allowable final DMSO concentration (1%), which has been reported to be well tolerated in zebrafish embryo assays [39,40]. Based on the concentration range identified in the initial screening, experiments were subsequently performed using 10 embryos per concentration in duplicate. E3 medium served as the negative control. The assay plates were incubated at 27.5 ± 0.5 °C (Phoenix Instrument TININ35, Naperville, IL, USA). Mortality was assessed at 120 h post-fertilization (hpf) using an Olympus CKX41 inverted microscope, equipped with a Leica EC3 digital camera and LAS EZ 3.2.0 software.

3.5.3. In silico profiling

The ADME properties of the synthesized derivatives were predicted using the SwissADME web server [33]. Putative protein targets were predicted using the SwissTargetPrediction web server [34] and the commercial PASS software [35].

Ethical statement. Animal housing and spawning were conducted in aquaria units approved by the Croatian Ministry of Agriculture (HR-POK-023), in accordance with Directive 2010/63/EU [41]. All experiments in this study were performed on non-protected embryonal stages (up to 120 hpf), which do not require approval from animal welfare authorities.

3.5.3.1. Statistical analysis. Statistical analyses and data visualization were performed using GraphPad Prism version 8.0.2. Before LC_{50} determination, the measured values were log-transformed to improve data fitting. LC_{50} values for zebrafish toxicity were calculated by applying nonlinear regression with a four-parameter logistic model allowing for a variable slope. The 95% confidence intervals were determined using the profile likelihood approach. The quality of the model fit was assessed based on the coefficient of determination (R^2) along with an examination of residuals.

4. Conclusion

In summary, a series of halogenated quinolinone–aziridine hybrids (±)-**14**–**20** inspired by marinoaziridine scaffolds was synthesized through an eight-step convergent route featuring a key Johnson–Corey–Chaykovsky aziridination reaction between quinolinone-derived sulfur ylide **5′** and *N*-tosyl imines **6**–**12**. The fluorine substitution pattern exerted a pronounced influence on the stereochemical outcome of the reaction, leading to complete diastereoselectivity in two notable cases, with compound (±)-**17** obtained exclusively as the *cis* isomer and compound (±)-**19** exclusively as the *trans* isomer.

Biological evaluation revealed pronounced structure–activity relationships governed by both aziridine stereochemistry and fluorine substitution pattern. Several *cis* derivatives displayed enhanced selectivity toward MCF-7 breast cancer cells combined with no cytotoxicity toward HEK293T cells, whereas some *trans* analogues exhibited higher overall antiproliferative potency but lower selectivity. Comparative analysis of mono- and difluorinated derivatives further demonstrated that the position of fluorine substituents plays a more important role in determining biological activity than fluorine content alone.

Zebrafish embryotoxicity studies revealed marked stereochemistry-dependent effects and showed that antiproliferative selectivity and developmental toxicity are not directly correlated. In parallel, *in silico* target prediction suggested the possible involvement of proliferation-related signalling pathways, including kinase-associated targets, providing a preliminary mechanistic rationale for the observed biological effects.

Taken together, these findings demonstrate that the fluorine substitution pattern plays a decisive role in controlling the stereochemical outcome of the synthesis, while both fluorine positioning and aziridine stereochemistry strongly influence the biological profile of the resulting quinolinone-aziridine hybrids. Future studies will focus on the preparation of enantiomerically enriched derivatives and elucidation of the molecular mechanisms responsible for the observed stereochemistry-dependent biological activity.

CRediT authorship contribution statement

Anđela Buljan: Conceptualization, Data curation, Investigation, Methodology, Supervision, Writing – original draft. **Marija Renić:** Methodology. **Ana Čikoš:** Methodology, Validation, Writing – review & editing. **Višnja Stepanić:** Formal analysis, Software, Validation, Writing – review & editing. **Karolina Begić Biškup:** Formal analysis, Validation, Writing – original draft. **Mladen Paradžik:** Formal analysis, Investigation, Writing – original draft. **Marin Roje:** Conceptualization, Funding acquisition, Methodology, Supervision, Writing – review & editing.

Informed consent statement

Not applicable.

Institutional review board statement

Not applicable. All experiments were conducted on the non-protected embryonal stages (up to 96 hpf), which do not require permission by animal wel-fare commissions (Directive 2010/63/EU).

Funding

This study was supported by the Croatian Government and the European Union through the European Regional Development Fund—the Competitiveness and Cohesion Operational Programme (KK.01.1.1.01) through the project Bioprospecting of the Adriatic Sea (KK.01.1.1.01.0002) granted to The Scientific Centre of Excellence for Marine Bioprospecting — BioProCro.

Declaration of competing interests

The authors declare that they have no known competing financial interests or personal relationships that could have appeared to influence the work reported in this paper.

Acknowledgments

We would like to thank the Croatian Government and the European Union through the European Regional Development Fund—the Competitiveness and Cohesion Operational Programme (KK.01.1.1.01) for funding this research through the project Bioprospecting of the Adriatic Sea (KK.01.1.1.01.0002) granted to The Scientific Centre of Excellence for Marine Bioprospecting — BioProCro. We also thank the Center for NMR for recording spectra.

Appendix A. Supplementary data

Supplementary data to this article can be found online at https://doi.org/10.1016/j.ejmech.2026.119212.

Data availability

Data will be made available on request.

References

[1] D.J. Newman, G.M. Cragg, Natural products as sources of new drugs, J. Nat. Prod. 83 (2020) 770–803, https://doi.org/10.1021/acs.jnatprod.9b01285.
[2] A.L. Harvey, Natural products in drug discovery, Drug Discov. Today 13 (2008) 894–901, https://doi.org/10.1016/j.drudis.2008.07.004.
[3] T. Rodrigues, D. Reker, P. Schneider, G. Schneider, Counting on natural products, Nat. Chem. 8 (2016) 531–541, https://doi.org/10.1038/nchem.2479.
[4] A.G. Atanasov, B. Waltenberger, E.-M. Pferschy-Wenzig, T. Linder, C. Wawrosch, P. Uhrin, V. Temml, L. Wang, S. Schwaiger, E.H. Heiss, J.M. Rollinger, D. Schuster, J.M. Breuss, V. Bochkov, M.D. Mihovilovic, B. Kopp, R. Bauer, V.M. Dirsch, H. Stuppner, Discovery and resupply of pharmacologically active plant-derived natural products: a review, Biotechnol. Adv. 33 (2015) 1582–1614, https://doi.org/10.1016/j.biotechadv.2015.08.001.
[5] J.W.-H. Li, J.C. Vederas, Drug discovery and natural products, Science 325 (2009) 161–165, https://doi.org/10.1126/science.1168243.
[6] F.E. Koehn, G.T. Carter, The evolving role of natural products in drug discovery, Nat. Rev. Drug Discov. 4 (2005) 206–220, https://doi.org/10.1038/nrd1657.
[7] M.S. Butler, The role of natural product chemistry in drug discovery, J. Nat. Prod. 67 (2004) 2141–2153, https://doi.org/10.1021/np040106y.
[8] T.F. Molinski, D.S. Dalisay, S.L. Lievens, J.P. Saludes, Drug development from marine natural products, Nat. Rev. Drug Discov. 8 (2009) 69–85, https://doi.org/10.1038/nrd2487.
[9] K.C. Nicolaou, S.A. Snyder, The art and science of total synthesis, Angew. Chem. Int. Ed. 48 (2009) 3440–3482, https://doi.org/10.1002/anie.200802019.
[10] E.J. Corey, The logic of chemical synthesis, Chem. Soc. Rev. 17 (1988) 111–133, https://doi.org/10.1039/CS9881700111.
[11] A. Buljan, V. Stepanić, A. Čikoš, S. Babić Brčić, K. Bojanić, M. Roje, Total synthesis and biological profiling of putative (±)-Marinoaziridine B and (±)-N-Methyl marinoaziridine A, Mar. Drugs 22 (2024) 310.
[12] D. Tanner, Chiral aziridines, Angew. Chem. Int. Ed. 33 (1994) 599–619, https://doi.org/10.1002/anie.199405991.
[13] J.B. Sweeney, Aziridines: epoxides' ugly cousins? Chem. Soc. Rev. 31 (2002) 247–258, https://doi.org/10.1039/B001443K.
[14] X.E. Hu, Nucleophilic ring opening of aziridines, Tetrahedron 60 (2004) 2701–2743, https://doi.org/10.1016/j.tet.2004.01.042.
[15] I.D.G. Watson, L. Yu, A.K. Yudin, Advances in aziridine chemistry, Acc. Chem. Res. 39 (2006) 194–206, https://doi.org/10.1021/ar050038t.
[16] G.S. Singh, M. D'hooghe, N. De Kimpe, Aziridines in medicinal chemistry, Chem. Rev. 113 (2013) 1441–1498, https://doi.org/10.1021/cr300255b.
[17] J.P. Michael, Quinoline, quinazoline and acridone alkaloids, Nat. Prod. Rep. 25 (2008) 166–187, https://doi.org/10.1039/B612168N.
[18] R. Musiol, Quinoline-based compounds, Curr. Med. Chem. 17 (2010) 1960–1973, https://doi.org/10.2174/092986710791233965.
[19] O. Afzal, S. Kumar, M.R. Haider, M.R. Ali, R. Kumar, M. Jaggi, S. Bawa, A review on anticancer potential of bioactive heterocycle quinoline, Eur. J. Med. Chem. 97 (2015) 871–910, https://doi.org/10.1016/j.ejmech.2014.07.044.
[20] S. Purser, P.R. Moore, S. Swallow, V. Gouverneur, Fluorine in medicinal chemistry, Chem. Soc. Rev. 37 (2008) 320–330, https://doi.org/10.1039/B610213C.
[21] D. O'Hagan, Understanding organofluorine chemistry, Chem. Soc. Rev. 37 (2008) 308–319, https://doi.org/10.1039/B711844A.
[22] K. Müller, C. Faeh, F. Diederich, Fluorine in pharmaceuticals, Science 317 (2007) 1881–1886, https://doi.org/10.1126/science.1131943.
[23] N.A. Meanwell, Fluorine and fluorinated motifs in drug design, J. Med. Chem. 61 (2018) 5822–5880, https://doi.org/10.1021/acs.jmedchem.7b01788.
[24] E.P. Gillis, K.J. Eastman, M.D. Hill, D.J. Donnelly, N.A. Meanwell, Applications of fluorine in medicinal chemistry, J. Med. Chem. 58 (21) (2015) 8315–8359.
[25] Y. Zhou, J. Wang, Z. Gu, S. Wang, W. Zhu, J.L. Aceña, V.A. Soloshonok, K. Izawa, H. Liu, Next generation of fluorine-containing pharmaceuticals, Chem. Rev. 116 (2016) 422–518, https://doi.org/10.1021/acs.chemrev.5b00392.
[26] T.W. Greene, P.G.M. Wuts, Protective Groups in Organic Synthesis, fourth ed., Wiley, 2007.
[27] A.W. Johnson, E.J. Corey, M. Chaykovsky, Dimethyloxosulfonium methylide, J. Am. Chem. Soc. 84 (1962) 685–686.
[28] E. Fischer, L. Knorr, Ueber eine neue Bildungsweise von Chinolin-Derivaten. Ber. Dtsch, Chem. Ges. (19) (1886) 2441–2445.
[29] H.L. Riley, J.F. Morley, N.A.C. Friend, Selenium dioxide, a new oxidising agent. Part I. Its reaction with aldehydes and ketones, J. Chem. Soc. 0 (1932) 1875–1883.
[30] R. Appel, Tertiary phosphane/tetrachloromethane, a versatile reagent for chlorination, dehydration, and P–N linkage, Angew. Chem. Int. Ed. Engl. 14 (1975) 801–811.
[31] V.K. Aggarwal, J.P.H. Charment, C. Ciampi, J.M. Hornby, C.J. Obrien, G. Hynd, R. Parsons, Additions of stabilised and semi-stabilised sulfur ylides to tosyl protected imines: are they under kinetic or thermodynamic control? J. Chem. Soc. Perkin Trans. 1 (2001) 3159–3166.
[32] D.K. Wang, L.X. Dai, X.L. Hou, Lewis acid promoted aziridination of imines with semistabilized sulfonium ylides: highly stereoselective synthesis of vinyl-and ethynyl-aziridines, J. Chem. Soc. Chem. Commun. (1997) 1231–1232.
[33] A. Daina, O. Michielin, V. Zoete, SwissADME: a free web tool to evaluate pharmacokinetics, drug-likeness and medicinal chemistry friendliness of small molecules, Sci. Rep. 7 (2017) 42717.
[34] A. Daina, O. Michielin, V. Zoete, SwissTargetPrediction: updated data and new features for efficient prediction of protein targets of small molecules, Nucleic Acids Res. 47 (2019) W357–W364, https://doi.org/10.1093/nar/gkz382.
[35] D. Filimonov, V. Poroikov, Probabilistic approaches in activity prediction, in: A. Varnek, A. Tropsha (Eds.), Chemoinformatics Approaches to Virtual Screening, Royal Society of Chemistry, Cambridge, UK, 2008, pp. 182–216, https://doi.org/10.1039/9781847558879-00182.
[36] A. Buljan, M. Roje, Application of green chiral chromatography in enantioseparation of newly synthesized racemic marinoepoxides, Mar. Drugs 20 (2022) 530, https://doi.org/10.3390/md20080530.
[37] T. Mosmann, Rapid colorimetric assay for cellular growth and survival: application to proliferation and cytotoxicity assays, J. Immunol. Methods 65 (1983) 55–63, https://doi.org/10.1016/0022-1759(83)90303-4.
[38] OECD, Test No. 236: fish embryo acute toxicity (FET) test. OECD Guidelines for the Testing of Chemicals, Section 2, Organization for Economic Cooperation and Development, Paris, 2013.

[39] J. Hoyberghs, C. Bars, M. Ayuso, C. Van Ginneken, K. Foubert, S. Van Cruchten, DMSO concentrations up to 1% are safe to be used in the zebrafish embryo developmental toxicity assay, Frontiers in Toxicology 3 (2021) 804033, https://doi.org/10.3389/ftox.2021.804033.

[40] J. Maes, L. Verlooy, O.E. Buenafe, P.A.M. de Witte, C.V. Esguerra, A.D. Crawford, Evaluation of 14 organic solvents and carriers for screening applications in zebrafish embryos and larvae, PLoS One 7 (10) (2012) e43850, https://doi.org/10.1371/journal.pone.0043850.

[41] S. Babić, L. Čizmek, A. Maršavelski, O. Malev, M. Pflieger, I. Strunjak-Perović, N. Topić Popović, R. Čož-Rakovac, P. Trebše, Utilization of the zebrafish model to unravel the harmful effects of biomass burning during amazonian wildfires, Sci. Rep. 11 (2021) 2527.

Update

European Journal of Medicinal Chemistry
Volume 320, Issue , 15 December 2026, Page

DOI: https://doi.org/10.1016/j.ejmech.2026.119364

European Journal of Medicinal Chemistry 320 (2026) 119364

Contents lists available at ScienceDirect

European Journal of Medicinal Chemistry

journal homepage: www.elsevier.com/locate/ejmech

Corrigendum

Corrigendum to "Halogenated quinolinone–aziridines: Substituent-controlled diastereodivergent synthesis and geometry-dependent antiproliferative activity" [Eur. J. Med. Chem., 319 (2026)119212]

Anđela Buljan [a], Marija Renić [a], Ana Čikoš [b], Višnja Stepanić [c], Karolina Begić [d], Mladen Paradžik [e], Marin Roje [a,*]

[a] Laboratory for Chiral Technologies, Scientific Center of Excellence for Marine Bioprospecting-BioProCro, Ruđer Bošković Institute, Bijenička cesta 54, Zagreb, 10000, Croatia
[b] NMR Centre, Ruđer Bošković Institute, Bijenička cesta 54, Zagreb, 10000, Croatia
[c] Laboratory for Computational Biology and Translation, Division of Electronics, Ruđer Bošković Institute, Bijenička cesta 54, Zagreb, 10000, Croatia
[d] Laboratory for Aquaculture Biotechnology, Ruđer Bošković Institute, Bijenička cesta 54, Zagreb, 10000, Croatia
[e] Laboratory of Experimental Therapy, Ruđer Bošković Institute, Bijenička cesta 54, Zagreb, 10000, Croatia

The authors regret the incorrect text that was published in the paper due to an inadvertent error. The corrected and accurate text follows below.

Funding

This study was supported by the Croatian Government and the European Union, through the European Regional Development Fund – the Competitiveness and Cohesion Operational Program (PK.1.1.10), for funding this research through the project Sustainable Bioprospecting of Organisms from the Adriatic Sea for Innovative Natural Products (PK.1.1.10.0001) - BioProCro, granted to the Center of Research Excellence for Marine Bioprospecting.

Acknowledgments

The authors wish to thank the Croatian Government and the European Union, through the European Regional Development Fund – the Competitiveness and Cohesion Operational Program (PK.1.1.10), for funding this research through the project Sustainable Bioprospecting of Organisms from the Adriatic Sea for Innovative Natural Products (PK.1.1.10.0001) - BioProCro, granted to the Center of Research Excellence for Marine Bioprospecting.

The authors would like to apologise for any inconvenience caused.

DOI of original article: https://doi.org/10.1016/j.ejmech.2026.119212.

* Corresponding author. Laboratory for Chiral Technologies, Ruđer Bošković Institute, Department of Organic Chemistry and Biochemistry, Bijenička cesta 54, 10000, Zagreb, Croatia.

E-mail addresses: Andjela.Buljan@irb.hr (A. Buljan), Ana.Cikos@irb.hr (A. Čikoš), Visnja.Stepanic@irb.hr (V. Stepanić), Karolina.Begic@irb.hr (K. Begić), Mladen.Paradzik@irb.hr (M. Paradžik), Marin.Roje@irb.hr (M. Roje).

https://doi.org/10.1016/j.ejmech.2026.119364

Available online 26 September 2026

0223-5234/© 2026 The Author(s). Published by Elsevier Masson SAS. All rights are reserved, including those for text and data mining, AI training, and similar technologies.